Contents lists available at SciOpen

Food Science and Human Wellness

journal homepage: https://www.sciopen.com/journal/2097-0765

China Food Publishing Co.

PI3K/Akt/mTOR-mediated bidirectional regulation of ampelopsin from *Nekemias megalophylla* modulates autophagy and apoptosis in cervical cancer

Shiyi Xu[a,1], Siyu Liao[a,1], Juan Xi[b,c,1], Ling Gong[a], Xue Zou[a], Xiaoli Yang[a], Jiangxue Di[d,*], Xiuqiao Zhang[a,e,*], Chun Gui[a,b,*]

[a]School of Pharmacy, Hubei University of Chinese Medicine, Wuhan 430065, China
[b]Hubei Shizhen Laboratory, Wuhan 430061, China
[c]School of Laboratory Medicine, Hubei University of Chinese Medicine, Wuhan 430065, China
[d]School of Management, Hubei University of Chinese Medicine, Wuhan 430056, China
[e]Hubei Provincial Key Laboratory for Chinese Medicine Resources and Chinese Medicine Chemistry, Hubei University of Chinese Medicine, Wuhan 430065, China

ARTICLE INFO

Article history:
Received 8 April 2024
Received in revised form 26 April 2024
Accepted 7 August 2024

Keywords:
Ampelopsin
Apoptosis
Autophagy
C-33A cell
PI3K/Akt/mTOR
Bidirectional regulation

ABSTRACT

Nekemias megalophylla is a popular folk tea consumed by people in the Western Hubei (China) of which ampelopsin (AMP) is the main active ingredient. In this study, we investigated the effect of AMP on cervical cancer and explored its mechanism of action, focusing on apoptosis and autophagy. Firstly, we verified that AMP strongly inhibited the growth of C-33A cells and observed apoptosis and autophagy phenomenon *in vivo*, and found that AMP induces C-33A cell apoptosis *via* death receptor or mitochondrial pathways. The results also indicated that AMP-induced autophagy occurs *via* the PI3K/Akt/mTOR pathway. Secondly, when autophagy was inhibited, the AMP-induced apoptosis of C-33A cells was strengthened, when apoptosis was inhibited, the AMP-induced autophagy of C-33A cells was strengthened. PI3K/Akt/mTOR pathway activation enhances AMP-induced apoptosis in C-33A cells, while its inhibition strengthens AMP-induced autophagy. Finally, we confirmed that AMP inhibited cell growth and induced apoptosis and autophagy of C-33A cells in an *in vivo* nude mouse model of C-33A tumor xenografts. These results elucidate that AMP bidirectionally regulates apoptosis and autophagy in human cervical cancer C-33A cells by mediating the PI3K/Akt/mTOR pathway.

© 2026 Beijing Academy of Food Sciences. Publishing services by Tsinghua University Press.
This is an open access article under the CC BY-NC-ND license
(http://creativecommons.org/licenses/by-nc-nd/4.0/).

1. Introduction

Cervical cancer (CC) is one of the most common and high-risk malignant tumors in women worldwide[1]. Over the past decades, the morbidity of CC has decreased in developed countries owing to vaccines and advanced diagnosis technology[2]. However, these numbers remain stubbornly high in developing countries, owing to the uneven distribution of medical resources and unadvanced testing techniques[3]. At the same time, the incidence of CC has increased in younger ages, mainly because of premature sexual intercourse, smoking, taking emergency contraception perennially, uterine dysplasia or other factors[4-5], as is the case in China[6]. To sum up, CC remains a severe threat to women's lives worldwide, so the development of effective drugs for CC is imperative.

Traditional chemotherapy and targeted drugs are the main treatment options for CC[7]. However, they have disadvantages, such as poor specificity, major side effects, and drug resistance. The potential of natural medicines as new anticancer drugs has been receiving increasing attention. Currently, more than 60% of the clinically used anticancer chemotherapeutic drugs were originally isolated from

[1] These authors contributed equally to this work.
[*] Corresponding authors.
E-mail address: 3001@hbtcm.edu.cn (C. Gui); 1445@hbtcm.edu.cn (X.Q. Zhang); 791424893@qq.com (J.X. Di)
Peer review under responsibility of Beijing Academy of Food Sciences.

SciOpen Publishing services by Tsinghua University Press

http://doi.org/10.26599/FSHW.2024.9250359
2213-4530/© 2026 Beijing Academy of Food Sciences. Publishing services by Tsinghua University Press. This is an open access article under the CC BY-NC-ND license (http://creativecommons.org/licenses/by-nc-nd/4.0/).

natural products[8], such as paclitaxel, camptothecins, and vinblastine[9]. Research studies on the natural medicinal ingredients of CC therapeutic drugs, including flavonoids, polysaccharides, saponins and alkaloids, have gradually increased[10]. For example, triptolide promotes apoptosis and autophagy by regulating the p53 pathway in HeLa cells[11]. *Rosa rugosa* polysaccharides can induce cervical cancer cell autophagy and apoptosis *via* PI3K/mTOR signaling pathway[12]. Icariin induces reactive oxygen species (ROS) production and reduces matrix metalloproteinase levels to block the mTOR/PI3K/Akt signaling cascade, ultimately inducing autophagy and apoptosis in HeLa and HCvEpC cells[13]. Licochalcone A induces cell apoptosis, inhibits PI3K/Akt/mTOR signaling, and leads to autophagy in SiHa and HeLa[14]. Therefore, finding high-efficiency and low-toxicity natural medicines for CC is a difficult task but a promising research topic.

Nekemias megalophylla (Diels & Gilg) J. Wen & Z. L. Nie is an ethnic medicinal plant of the genus *Ampelopsis* belong to family Vitaceae. It is widely used as a popular vine tea in South China, with at least 35 aliases in 10 provinces. People use dried tender stems and leaves of *N. megalophylla* to make tea to help strengthen the body, which is very popular in areas where *N. megalophylla* tea is consumed[15]. Dihydromyricetin, also known as ampelopsin (AMP, Fig. 1A), is the main active ingredient derived from *N. megalophylla.*

Our team has been studying the anti-CC activity of AMP and its mechanism[16-18]. AMP is a small molecule flavonoid compound with increasing potential as a natural anticancer drug that is safe, non-toxic, and does not elicit cross-resistance. AMP has been reported to show growth-inhibitory effects on different types of human cancers, such as gastric, breast, liver, lung, ovarian, colon, choriocarcinoma, and osteosarcoma[19]. For instance, AMP has been shown to inhibit human cholangiocarcinoma tumor growth *via* miRNA-455-3p[20]. Zhao et al.[21] suggested that AMP prevents the growth of renal cancer cells by inhibiting the PI3K/Akt signaling pathway. However, the effects of AMP on CC and its underlying mechanisms have not been reported, except by our team, thus requiring further investigation.

Our previous research found that AMP induced apoptosis in HeLa, SiHa, and C-33A cells, with the highest inhibitory rate in C-33A cells[16-17]. Therefore, to explore the mechanisms underlying these beneficial effects of AMP, we studied apoptosis and autophagy *in vitro* and *in vivo*. Apoptosis and autophagy correlation was investigated through co-treatment with AMP and apoptosis or autophagy inhibitors *in vitro*. A nude mouse model of C-33A tumor xenografts was established to confirm and consolidate the previous results *in vivo*. This study will lay the foundation for creating and clinically applying new cervical cancer drugs with specific targets and promote the use of medicinal resources and economic development in Western Hubei of China.

2. Materials and methods

2.1 Reagents and antibodies

AMP (≥ 98% purity) was extracted and isolated from *N. megalophylla* as previously described by our group[21]. Cisplatin (DDP, #B21M11L110000) was purchased from Yuanye (Shanghai, China), MEM (Minimum Eagle Medium) was purchased from Procell (Wuhan, China).

Antibodies p-Akt (#4060s), Akt (#4691S), Bcl-2 (#4223S), Bax (#5023S), Atg5 (#12994T), Atg13 (#13273S), cleaved-Caspase 3 (#9664S), cleaved-PARP (#5625S), GAPDH (#8884S), p62 (#39749S), Beclin 1 (#3495S), p-mTOR (#5536s) and mTOR (#2983S)

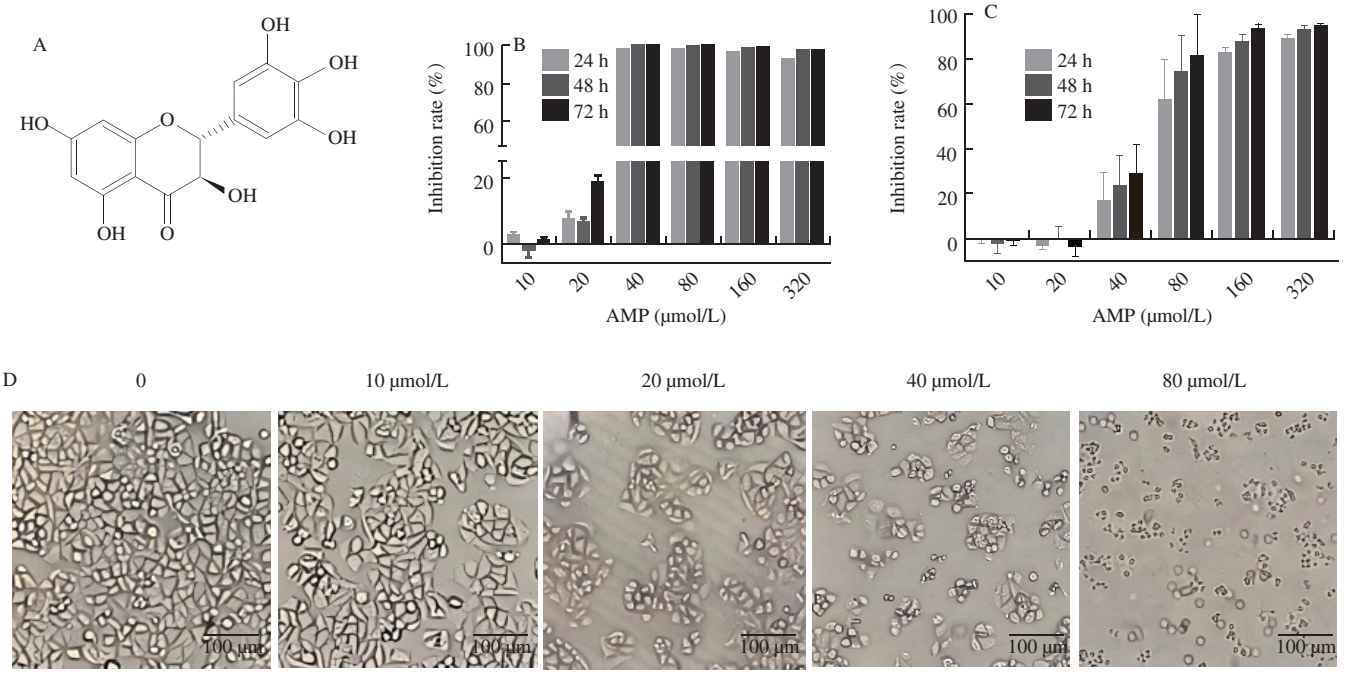

Fig. 1 AMP inhibits cervical cancer cell proliferation. (A) AMP structure. (B-C) The MTT assay was employed to test inhibition rate of (B) C-33A and (C) SiHa cells. Cells were treated with AMP (0, 10, 20, 40, 80, 160, and 320 μmol/L) for 24, 48, and 72 h, respectively. (D-E) Preliminary morphological features of C-33A cells were observed under a light microscope. (F-G) Preliminary morphological features of SiHa cells were observed under a light microscope. Cells were exposed to AMP (0, 10, 20, 40, and 80 μmol/L) for 12 h or 40 μmol/L AMP treated for 6, 12, 24, and 48 h, respectively. Scale bar: 100 μm. Data are represented as the mean ± SD, $n = 3$.

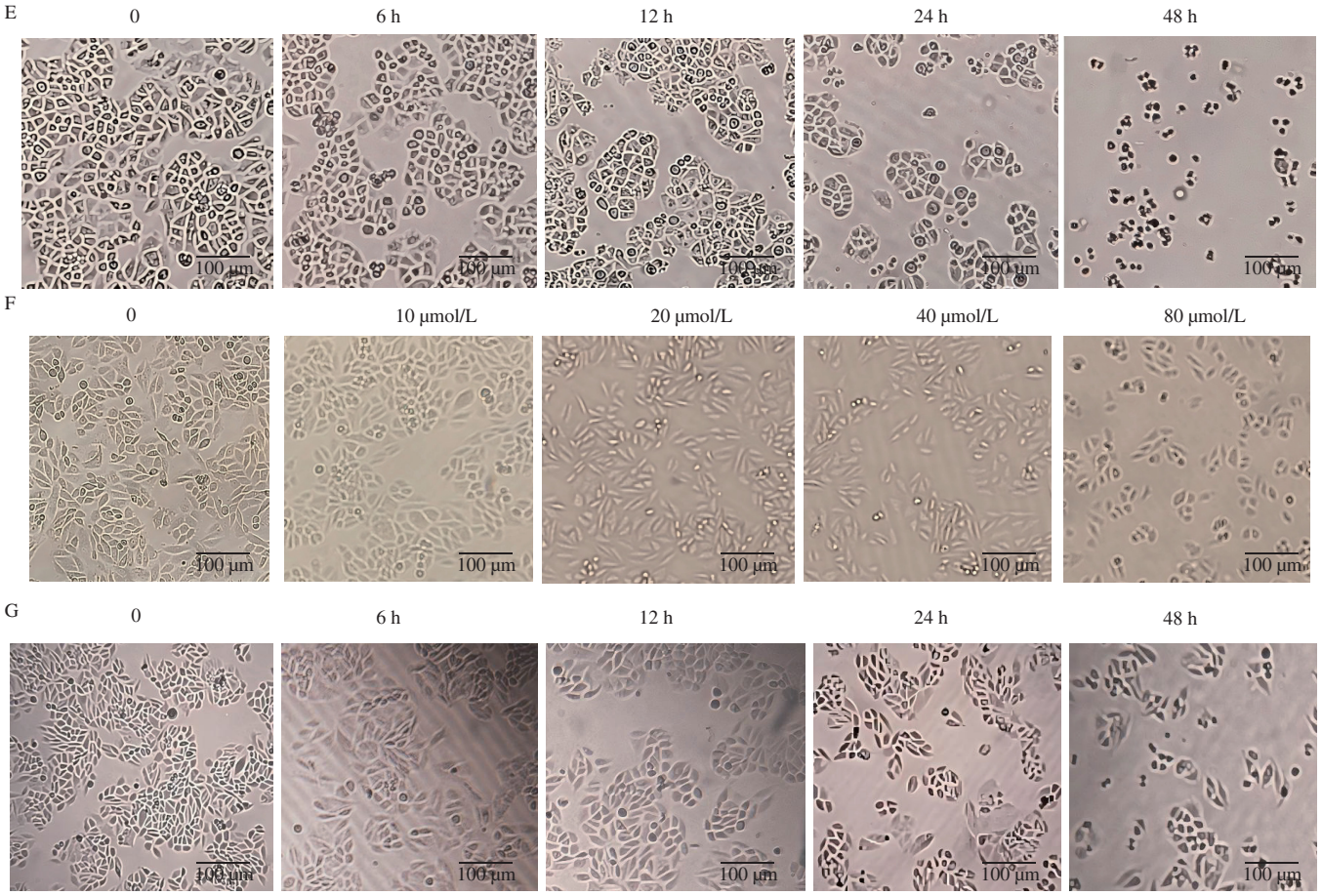

Fig. 1 (*Continued*)

were purchased from CST (MA, USA). Antibodies Cyt-c (#A13430), Caspase 3 (#A2156), and FADD (#A5819) were obtained from ABclonal (Wuhan, China). Antibodies p-PI3K (#182651) and PI3K (#ab190616), goat anti-rabbit IgG H&L (#ab6721) were acquired from Abcam (Cambridge, UK). Antibodies LC3 (#14600-1-AP) and PARP (#A23000247) were obtained from Proteintech (Wuhan, China). Z-VAD-FMK and 3-methyladenine (3-MA) were obtained from the Meilunbio Co. (Dalian, China). Lysosome(#C1047S) and DAPI (#111622230510) were purchased from Beyotime (Shanghai, China). TNF-α (#EK0527), IL-2 (#EK0398), IL-1β (#EK0394) and IL-6 (#EK0411) were purchased from BOSTER (Wuhan, China).

2.2 Cell line and culture

The C-33A and SiHa cell lines were acquired from the Cell Culture Center of the Shanghai Institute of Biological Sciences (#CL0045, #CL0210, Wuhan, China) and cultured in MEM medium (Procell, Wuhan, China) including 10% fetal bovine serum (FBS, #42G4084K, Gibco, USA) in a constant-temperature incubator (37 ℃) (Galaxy s+, RS Biotech, UK) with 5% CO_2.

2.3 Cell proliferation assay

Effect of AMP in C-33A cells and SiHa were detected by 3-(4,5-dimethyl-2-thiazolyl)-2,5-diphenyl-2-*H*-tetrazolium bromide assay (MTT) (#M-2128, Awresco, USA) assay. Briefly, cells were seeded in 96-well plates with 5×10^3 cells/well and treated with different drugs. Then, 20 μL of MTT reagent was added and cultured for 4 h. Next, poured the old MEM medium away, DMSO was added. The optical density (OD) of the cells was measured using a microplate reader (Bio-Rad, US). Each experiment was repeated 3 times. The growth inhibition rate was calculated as follows:

$$\text{Inhibition rate (\%)} = \frac{OD_{control} - OD_{drug\ group}}{OD_{control}} \times 100 \quad (1)$$

2.4 Hoechst 33258 staining

Cells were seeded in 6-well plates and treated with the different drug groups for the defined treatment time for each condition. After treatment, methanol/glacial acetic acid (3:1) was used to fixed cells at 25 ℃ for 13 min. Next, 5 μg/mL Hoechst 33258 (#Novazan, Nanjing, China) was used to stain cells in the dark. The morphological features were observed and recorded under a fluorescence microscope (IX51, Olympus, Japan).

2.5 Annexin V-FITC/PI double staining

The cells apoptosis rate was tested by Annexin V-FITC/PI (#A211-01, Novazan, Nanjing, China) double staining kit. Cells were collected and washed after exposure to each treatment. Subsequently, 5 μL Annexin V-FITC and 5 μL PI were stained for 5 min each. Finally, all samples were analyzed *via* flow cytometry (FCM, FACSCalibur, USA).

2.6 Western blot analysis

Firstly, cells were seeded in culture dishes and exposed to the different drugs for different durations according to the specific experiments. Secondly, abandoned the old medium, broken cells, centrifuged, got the supernatant and detected the concentration. Then, each protein sample was run on SDS-PAGE gels and electrically transferred to the polyvinylidene difluoride membranes (PVDF, Merck, Germany). After transfer, the membranes were blocked with a 5% skim milk powder solution for 1.5 h. The primary antibody was incubated for the night, and then with the corresponding the secondary antibody for 1 h. Finally, enhanced chemiluminescence (Meilunbio, Dalian, China) was used to visualize protein bands. ImageJ v 1.48 and SPSS 23.0 software were used for quantitative analysis.

2.7 Monodansylcadaverine (MDC) staining

C-33A cells were seeded in confocal dishes with 1.0×10^5 per well. Each well was treated as per the corresponding drug groups, poured the old MEM medium away, and cells were dyed with 50 μmol/L MDC (#BCBX0277, Sigma, USA) for 40 min in an incubator. Autophagosomes were observed by a confocal microscope (FV3000, Olympus, Japan).

2.8 Transmission electron microscopy (TEM) analysis

C-33A cells were cultured and treated according to each experiment, and TEM (Tecnai G^2 20 TWIN, FEI, USA) observation was performed. The cells were then fixed in an electron microscope fixture and with a phosphate solution (0.1 mol/L) for 2 h. After fixation, the cells were embedded in a mixture of acetone and an embedding agent. Ultrathin sections were stained with 2% uranium acetate and dissolved in saturated alcohol. The cell ultrastructure was observed and photographed using a TEM.

2.9 Autophagic flux assay

Cells were seeded in 6-well plates with 4.0×10^5 per well and maintained in serum-free MEM. The cells were then transfected with mRFP-GFP-LC3 adenovirus (#AP20102304, Hansheng, Shanghai, China) before treatment with different AMP concentrations for 12 h. After incubation, those samples were fixed with 4% paraformaldehyde for 20 min and observed under a laser confocal microscope (LSM880, ZEISS, Germany). Green GFP fluorescence indicates the perence of the autophagic marker protein LC3, while red mRFP fluorescence indicates the number of autophagic lysosomes, and yellow merged areas represent autophagosomes.

2.10 Immunofluorescence (IF) assay

The cells were inoculated in confocal laser culture dishes treated with 0.01% polylysine, and were administered in groups and cultured for 24 h. Medicated medium was removed, fixed with 4% paraformaldehyde for 15 min, sealed with 1% BSA for 1 h, LC3 antibody diluted with 3% BSA was added, and incubated at 4 ℃ overnight. Then, Cy3 fluorescent secondary antibody diluted with 3% BSA was added and incubated for 1 h away from light. The Lysosome dyeing solution prepared in advance was added and incubated at 37 ℃ for 1 h. Finally, add DAPI dye solution and dye at 37 ℃ for 3 min away from light. After the sealing of the anti-fluorescence attenuation tablet, a laser confocal microscope (#FV300, Olympus, Japan) was used to take pictures and record the magnification of 1 000 times. The LC3 protein was fluorescently labeled with Cy3 red, and the fluorescence secondary antibody excitation wavelength was 550 nm, and the emission wavelength was 570 nm. Green fluorescent labeling of lysosomes, DAPI blue fluorescent label cell nucleus, DAPI dye solution and DNA binding excitation wavelength of 364 nm, emission wavelength of 454 nm.

2.11 Animal studies

Approximately 4-week-old female BALB/c nude mice were purchased from Hangzhou Ziyuan Animal Experiment Technology Co., Ltd. (#SCXK (ZHE) 2019-0004, Hangzhou, China). After a 7-day adaptation period, a suspension of C-33A cells (1×10^7 cells/mouse) was rapidly injected into the right subcutaneous tissue of the mice. The mice were then observed, and their weights were record every 3 days for 2 weeks. When the subcutaneous tumor reached a volume 60 mm^3, all mice were randomized to 4 groups: the control, low-AMP (50 mg/kg AMP), high-AMP (200 mg/kg AMP), and positive (2.5 mg/kg DDP) group (n = 6 mice per group). The 2 AMP groups were intraperitoneally injected with the corresponding does of AMP and the control group was injected with saline every day, the DDP group was injected intraperitoneally with the indicated does of DDP twice a week. We also measured the tumor length, width, and mouse weight on days 1, 4, 7, 10, 13, 16, 19, and 22. On day 23, the blood from the mice was collected for ELISA analysis, and the dissected tumors and organ tissues were weighed, photographed, and stored in a general-purpose tissue fixative solution (#G1101, Saywell, Wuhan, China) for western blot or RT-qPCR analysis. Some tumor tissues were fixed in an electron microscope fixture for TEM.

Tumor volume was calculated as equation (2):

$$\text{Volume } (mm^3) = \frac{\text{length} \times \text{width}^2}{2} \quad (2)$$

Organ coefficient was calculated as equation (3):

$$\text{Organ coefficient } (\%) = \frac{\text{Organ weight}}{\text{Mouse body weight}} \times 100 \quad (3)$$

2.12 Enzyme-linked immunosorbent assay (ELISA) analysis

The levels of TNF-α, IL-6, IL-2, and IL-1β were detected using an ELISA kit (BOSTER, Wuhan, China). All procedures were performed to following the manufacturer's instructions.

2.13 Quantitative real-time PCR (RT-qPCR) analysis

Tumor Xenografts from each group were used to extract the total RNA. RNA was extraced following the intructions of an NRAprep pure tissue kit (#U9124, DP451, Tiangen, Beijing, China). cDNA was reverse-transcribed using the a PrimeScript™ RT reagent kit with gDNA Eraser (perfect Real Time) (#AK716484A, RR047A, TAKARA, Japan). A TB Green™ Premix Ex Taq™ II (Tli RNaseH

Plus) kit (#AK51600A, RR820A, TAKARA, Japan) was employed for quantitative RT-PCR using an RT-PCR instrument (StepOnePlus, Applied Biosystems, USA).

Primer sequences as follows. *Bax*: forward primer (5'-3'), TGCTTCAGGGTTTCATCCAG; reverse primer (5'-3'), GGCGGCAATCATCCTCTG. *Bcl-2*: forward primer (5'-3'), TACGAGTGGGATGCGGGAGATG; reverse primer (5'-3'), CCGGGCTGGGAGGAGAAGATG. *Beclin 1*: forward primer (5'-3'), AGCTGCCGTTATACTGTTCTG; reverse primer (5'-3'), ACTGCCTCCTGTGTCTTCAATCTT. *LC3 II*: forward primer (5'-3'), GCAGGGTAAACGGGCTGTGTG; reverse primer (5'-3'), GAGTGAGGACTTTGGGTGTGGTTC. *GAPDH*: forward primer (5'-3'), GTTTGTGATGGGTGTGAACC; reverse primer (5'-3'), TCTTCTGAGTGGCAGTGATG.

2.14 Statistical analysis

All data are expressed as the mean ± standard deviation (SD). Comparisons among multiple data were performed using one-way ANOVA in SPSS software 23.0. Protein levels were quantified by Image-Pro Plus 6.0 software. $P < 0.05$ was considered statistically significant.

3. Results

3.1 AMP inhibits cervical cancer cell proliferation

C-33A or SiHa cells were intervened with AMP (0, 10, 20, 40, 80, 160, and 320 μmol/L) for 24, 48, and 72 h, respectively. In Figs. 1B and C, the MTT assay suggested that AMP could remarkably inhibit the 2 CC cells growth, with half inhibition rates (IC_{50}) of C-33A cell were (22.96 ± 1.18), (21.32 ± 0.27) and (22.43 ± 0.63) μmol/L at 24, 48, and 72 h, respectively, the IC_{50} of SiHa cell were (80.90 ± 13.03), (70.00 ± 13.33) and (63.89 ± 8.91) μmol/L at 24, 48 and 72 h, respectively; Compared with the control group (Figs. 1D-G), morphological feature images showed a gradual decrease in the number of intact cells and the concomitant increase in the number of broken cells with increasing AMP concentration or exposure duration. These results suggest that AMP inhibits C-33A and SiHa cells proliferation.

At the same time, we found that while the dose of 40 μmol/L or higher of AMP treated to C-33A cells, already all cells proliferation were inhibited or even death. So, we explored the dose between 10–40 μmol/L for AMP to C-33A cell to show the inhibitory effect again (Fig. S1). The result found that the IC_{50} were (20.60 ± 0.94), (18.59 ± 0.61), and (22.10 ± 1.21) μmol/L at 24, 48, and 72 h, respectively, which showed a good inhibitory effect of AMP-treated C-33A cell. Therefore, these results suggest that AMP inhibits C-33A cell proliferation.

3.2 AMP induces apoptosis in cervical cancer cells

C-33A cells were exposed to AMP (0, 10, 20, 40, and 80 μmol/L) for 12 h or 40 μmol/L AMP treated cells for 0, 6, 12, and 24 h. Hoechst 33258 staining displayed that the number of cells gradually decreased and shrank with the increasing in AMP concentration or exposure duration, compared with the control group (Figs. 2A and B). Annexin V-FITC/PI staining revealed an increasing apoptosis rate depending on AMP concentration, from (7.31 ± 0.50)% to (71.16 ± 11.10)% in the concentration range of 0–80 μmol/L. Furthermore, the apoptosis rate also increased from (7.02 ± 1.67)% to (58.86 ± 10.66)% when cells were exposed to AMP (40 μmol/L) for 6, 12, and 24 h, respectively (Figs. 2C and D). Meanwhile, SiHa cells were exposed to AMP (0, 10, 20, 40, and 80 μmol/L) for 12 h to detect apoptosis rate. The apoptosis rate also increased from (2.58 ± 1.02)% to (23.10 ± 2.41)% (Fig. S2).

The levels of Bax/Bcl-2, cleaved-PARP/PARP, and cleaved-Caspase 3/Caspase 3 were found to be up-regulated (Figs. 2E and F). After treatment with the apoptosis inhibitor Z-VAD-FMK (50 μmol/L) (Fig. S3), we observed that these protein levels were down-regulated compared with AMP-treated cells. Thus, AMP inhibited C-33A cell growth through apoptosis induction.

We further explored the specific apoptotic pathways involved, using FADD and cytosolic Cyt-c, which are the represent of the 2 forms

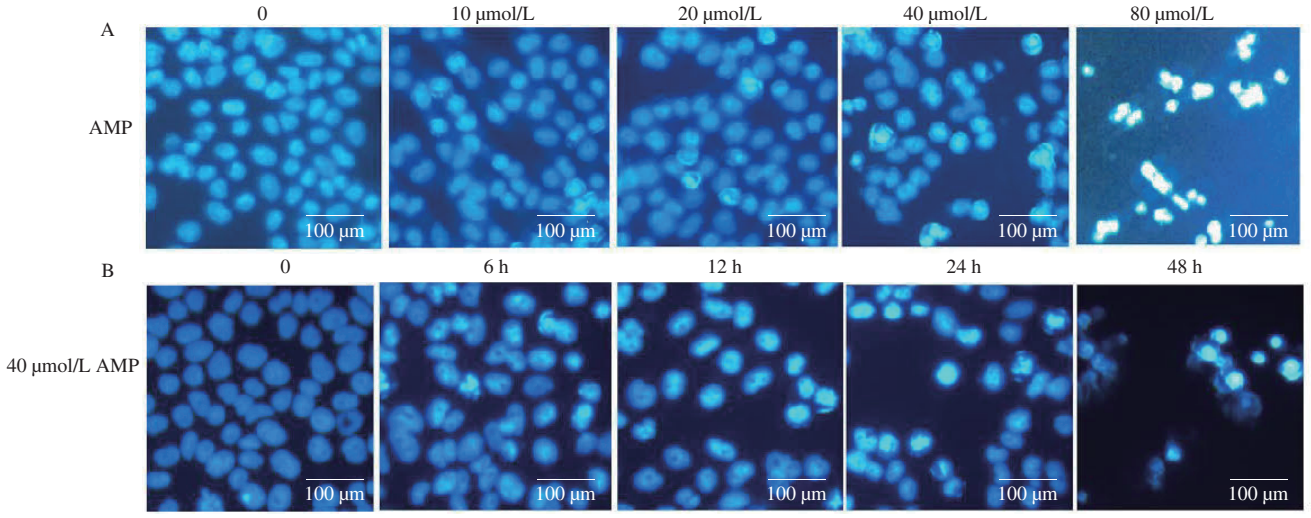

Fig. 2 AMP induces apoptosis in C-33A cells. Cells were exposed to AMP (0, 10, 20, 40, and 80 μmol/L) for 12 h or 40 μmol/L AMP for 0, 6, 12, and 24 h. (A-B) Hoechst 33258 staining was used to observe the typical morphological features of apoptotic cells using by a fluorescence microscope. Scale bar: 100 μm. (C-D) Annexin V-FITC/PI staining was used to analyze C-33A cell apoptosis. (E-F) Apoptotic proteins levels were evaluated using Western blot. Data are represented as mean ± SD, $n = 3$. *$P < 0.05$, **$P < 0.01$ *vs*. control. ns, not significant.

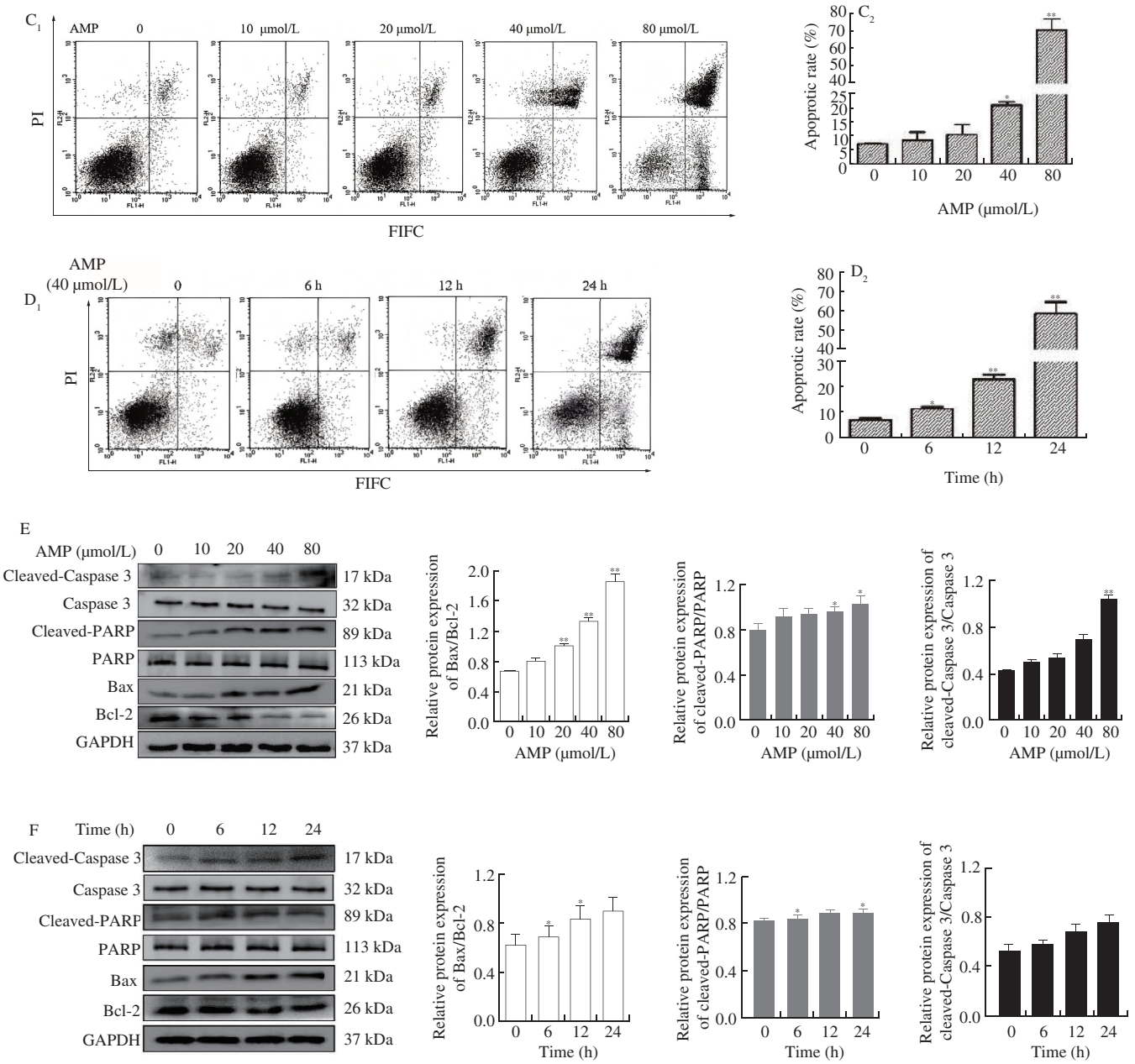

Fig. 2 (*Continued*)

of apoptosis[22-23]. As shown in Fig. 3A, the levels of FADD and cytosolic Cyt-c were up-regulated. When apoptosis was inhibited, AMP increased the levels of FADD and cytosolic Cyt-c (Fig. 3B), indicating that the mitochondrial or death receptor pathway was activated.

3.3 AMP induces autophagy in cervical cancer cells

MDC fluorescence staining was used to observe cell morphology during autophagy. C-33A cells were exposed to AMP (0, 10, 20, 40, and 80 μmol/L) for 12 h or to 40 μmol/L AMP for 0, 6, 12, and 24 h. Compared with the control group, the number of autophagosomes with bright green spots in C-33A cells gradually increasing with incremental AMP concentration or exposure duration (Figs. 4A and B).

TEM was used to observe the cell ultrastructures, such as the mitochondria, lysosomes, or autophagosomes in C-33A cells exposed to AMP (0 and 20 μmol/L) for 12 h. In Fig. 4C, no morphological changes were apparent in the control group. However, autophagosomes containing mitochondria and other organelles were detected in the AMP-treated group. Unexpectedly, shriveled nuclei were also observed in the AMP-treated group, which is an important apoptotic phenomenon.

Subsequently, the levels of the autophagic proteins LC3 II/LC3 I, Beclin 1, and p62 were analyzed. We observed an up-regulation of LC3 II/LC3 I and Beclin 1 expression and a downregulation of p62 expression dependent on AMP concentration or exposure duration (Figs. 4D and E). Cells were also exposed to the autophagy inhibitor 3-MA for 2 h prior to AMP treatment. Upon autophagy prevention, AMP decreased LC3 II/LC3 I, Beclin 1 levels and increased p62 levels (Fig. S4A), the level of AMP on autophagy gold marker LC3 protein and autophagy lysosome were decreased by IF (Fig. S4B). In

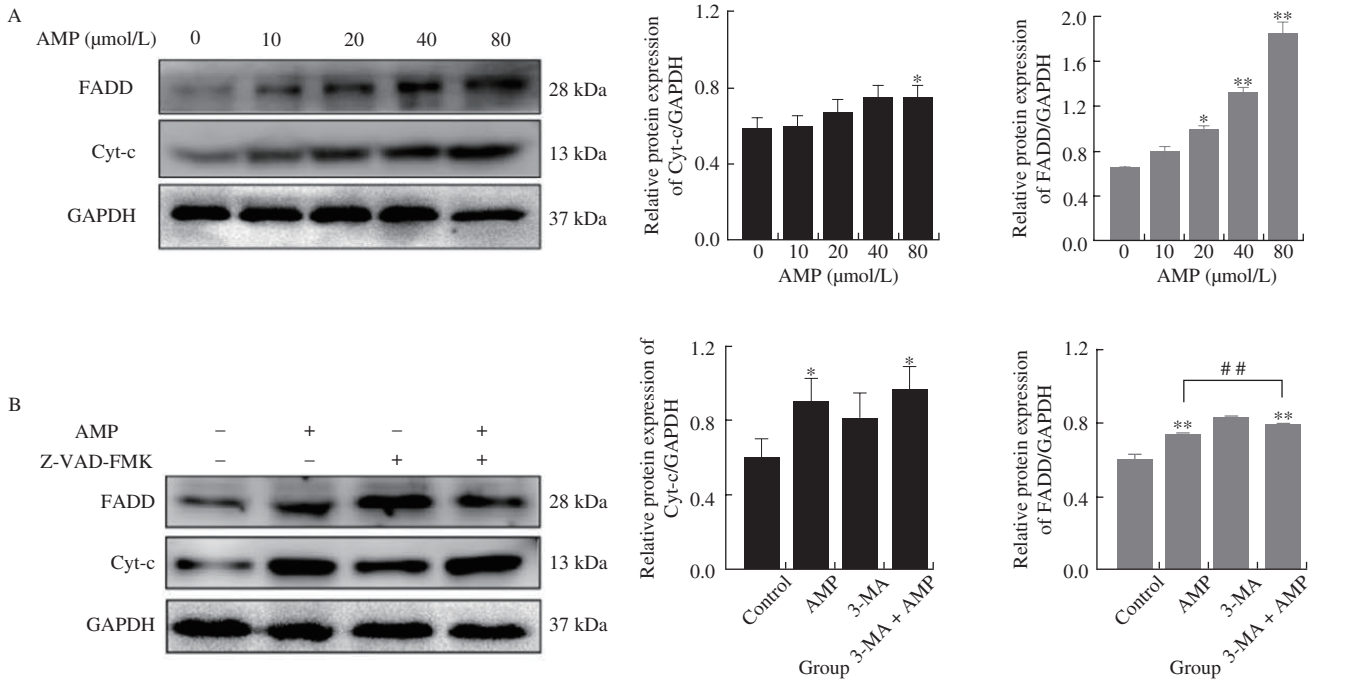

Fig. 3 AMP induces apoptosis in C-33A cells *via* 2 pathways. (A) Levels of FADD and cytosolic Cyt-c were determined in C-33A cells treated with AMP (0, 10, 20, 40, and 80 μmol/L) for 12 h. (B) Levels of FADD and cytosolic Cyt-c were evaluated in C-33A cells treated with AMP (40 μmol/L) and Z-VAD-FMK (50 μmol/L) *via* Western blot. Data are represented as the mean ± SD, $n = 3$. $^{*}P < 0.05$, $^{**}P < 0.01$ *vs*. control. $^{\#\#}P < 0.01$ *vs*. AMP. ns, not significant.

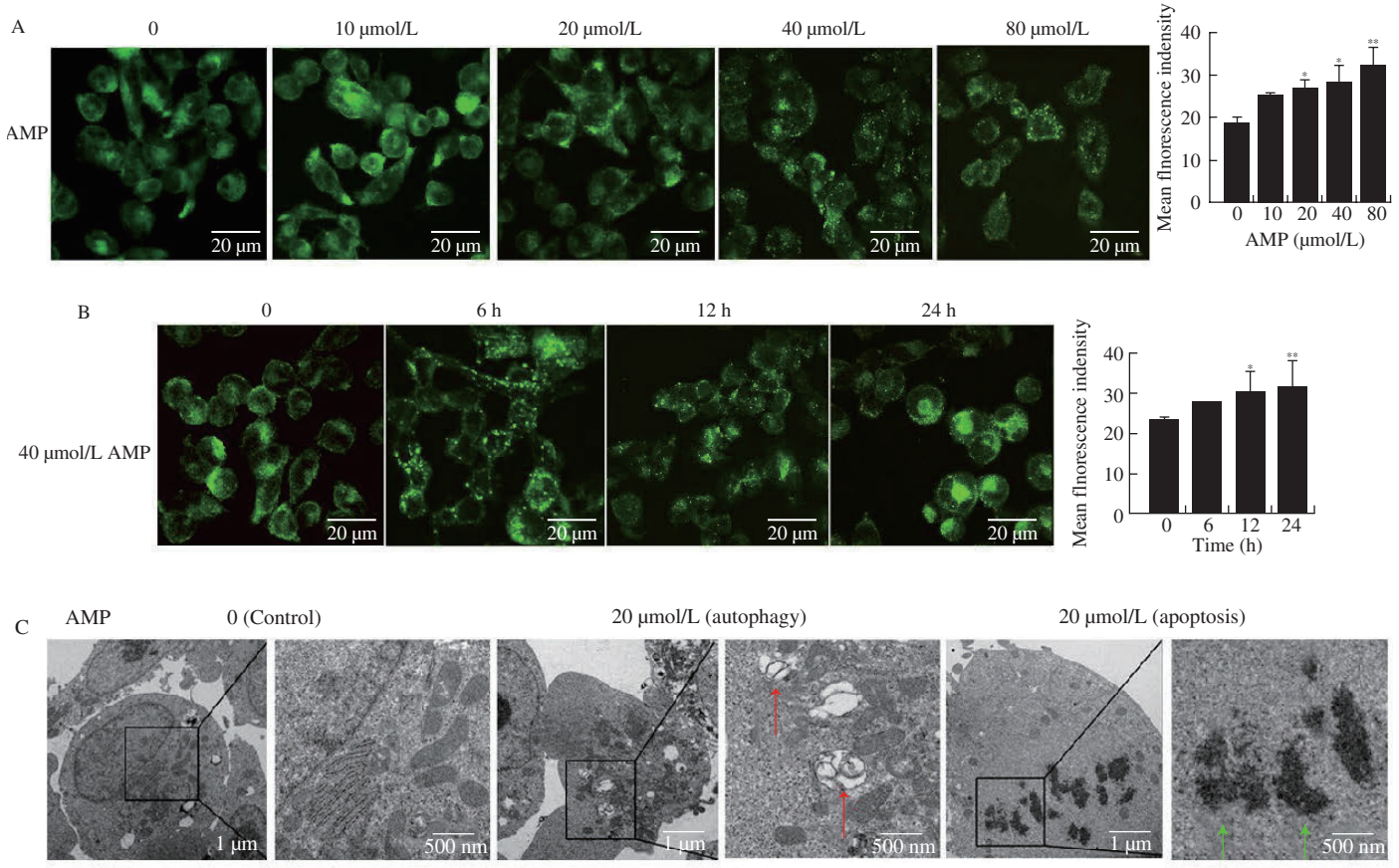

Fig. 4 AMP induces autophagy in C-33A cells. (A, B) Preliminary morphological features of autophagic cells were observed under a confocal microscope after MDC dyeing. Cells were treated with AMP (0, 10, 20, 40, and 80 μmol/L) for 12 h or AMP (40 μmol/L) for 0, 6, 12, 24 h. Scale bar: 20 μm. (C) Typical cell ultrastructure of autophagic cells was observed using TEM. C-33A cells were treated with AMP (0 and 20 μmol/L) for 12 h. Scale bars: 1 μm or 500 nm. (D, E) Levels of LC3 I, LC3 II, Beclin 1 and p62 were determined by Western blot. The concentrations of AMP were the same in (A) and (B). Data are represented as the mean ± SD, $n = 3$. $^{*}P < 0.05$, $^{**}P < 0.01$ *vs*. control. ns, not significant.

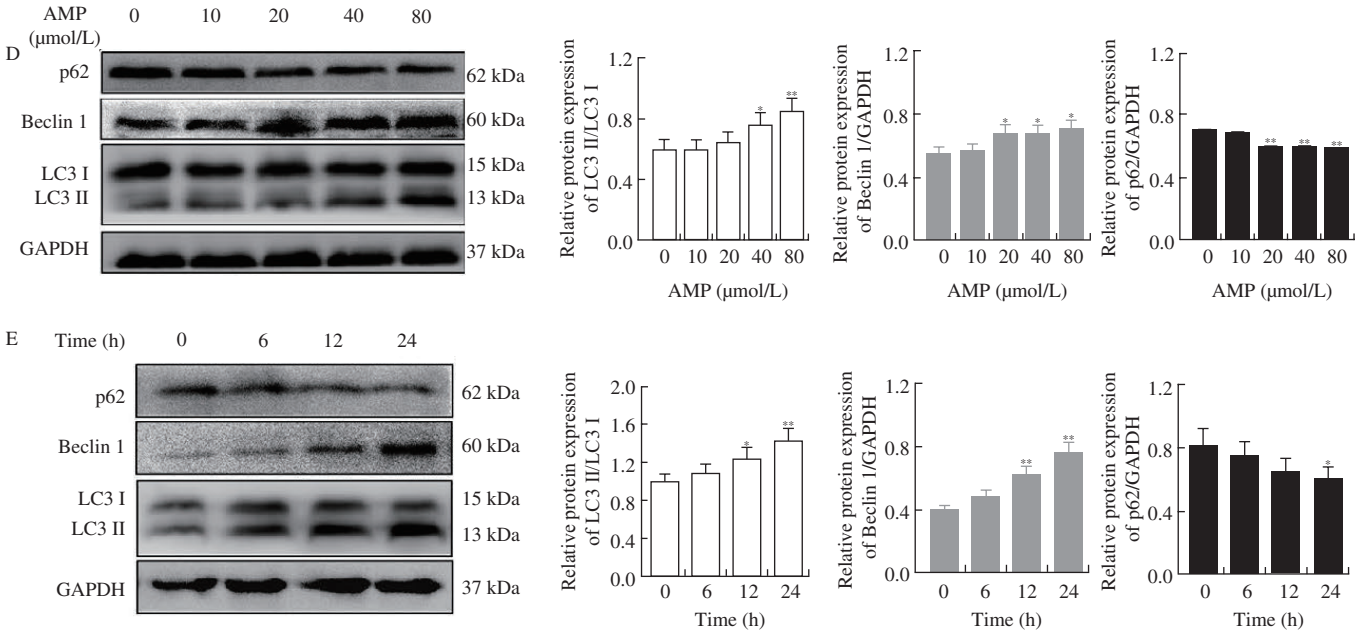

Fig. 4 (*Continued*)

accordance with the AMP-driven autophagy promotion tested, Atg5 and Atg13 were up-regulated with increasing AMP concentration or exposure duration (Figs. 5A and B).

Since autophagy is a dynamic process[24], we evaluated autophagy flux using transfection with an autophagy double-labeled lentivirus (mRFP-GFP-LC3). C-33A or SiHa cells were transduced with these lentiviruses and exposed to AMP (0, 20, 40, and 80 μmol/L) for 12 h. The number of green fluorescent spots decreased, while those of the red and yellow fluorescent spots increased for the 2 cells (Figs. 5C and F), indicating that autolysosomes and autophagosomes increased in intensity (Figs. 5D and G) and, consequently, the enhancement of the autophagy flux (Figs. 5 E and H).

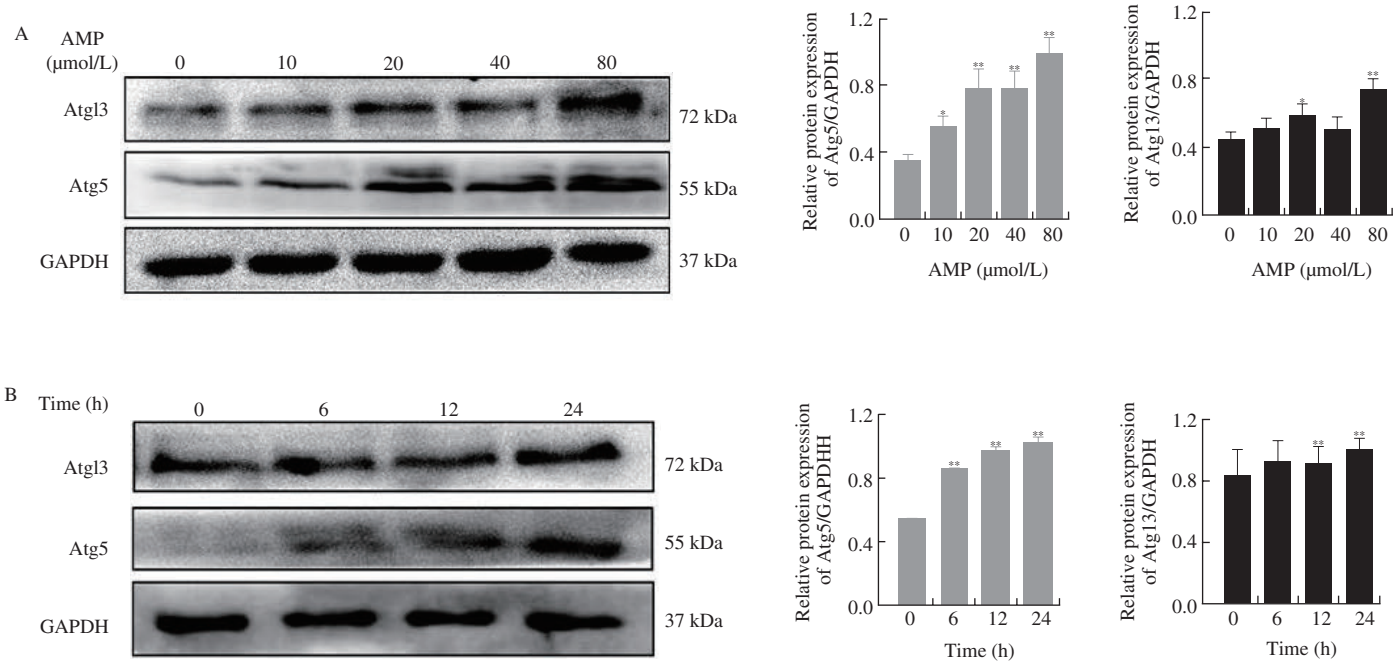

Fig. 5 AMP induces autophagy in C-33A cells. (A) Levels of Atg-related proteins in C-33A cells treated with AMP (0, 10, 20, 40 and 80 μmol/L) for 12 h. (B) Levels of Atg-related proteins in C-33A cells treated with AMP (40 μmol/L) for 0, 6, 12, 24 h. (C, F) Autophagy flux level was examined after mRFP-GFP-LC3 transfection. C-33A or SiHa cells were exposed to AMP (0, 20, 40, 80 μmol/L) for 12 h. Green GFP fluorescence indicates the LC3 protein, red mRFP fluorescence indicates autophagic lysosomes, and yellow merge fluorescence refers to autophagosomes. Scale bar: 20 μm. (D, G) Quantitative analysis of the fluorescence intensity of mRFP or GFP fluorescence. (E, H) Quantitative analysis of the fluorescence co-localization ratio (MOC). Data are represented as the mean ± SD, $n = 3$. *$P < 0.05$; **$P < 0.01$, *vs*. control. ns, not significant.

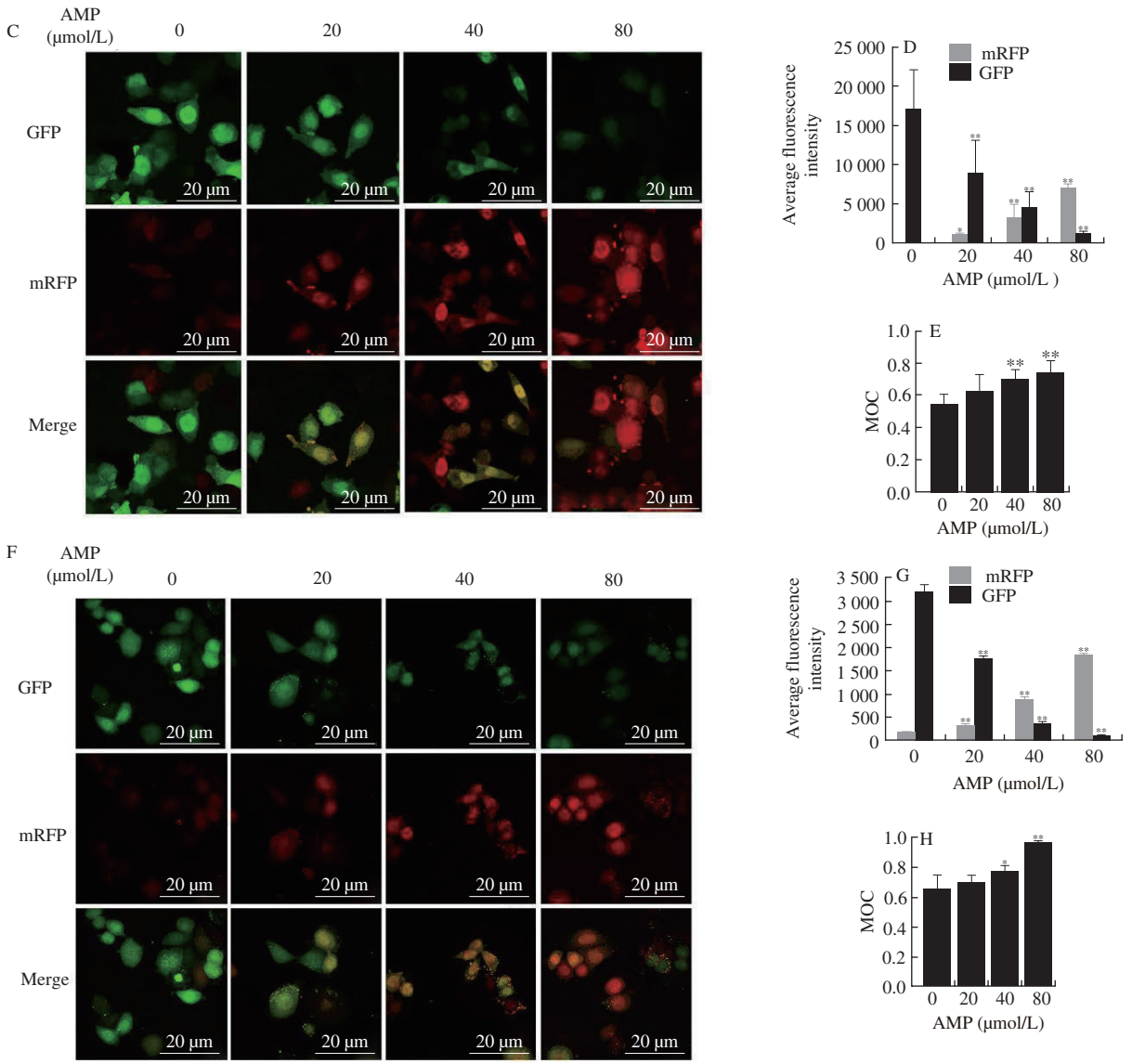

Fig. 5 (*Continued*)

3.4 AMP induces autophagy in C-33A cells via the PI3K/Akt/mTOR signaling pathway

The most classic and significant autophagy-related signaling pathway is the PI3K/Akt/mTOR pathway. Upon AMP treatment, the total levels of PI3K, Akt, and mTOR remained unchanged, but their phosphorylated forms, p-PI3K, p-Akt, and p-mTOR, respectively, were down-regulated (Figs. 6A and B).

3.5 Interaction of apoptosis and autophagy on AMP-induced C-33A cell death

3.5.1 AMP combined with inhibitors to intervene in C-33A cell growth

In this study, 3-MA and Z-VAD-FMK were the inhibitors selected to investigate the association between autophagy and apoptosis. Six groups were established: control, AMP, 3-MA, 3-MA combined with AMP (3-MA + AMP), Z-VAD-FMK, and Z-VAD-FMK combined with AMP (Z-VAD-FMK + AMP). The cells were first exposed to 3-MA (5 mmol/L) or Z-VAD-FMK (50 μmol/L) for 2 h, then AMP (40 μmol/L) was then added to the combination groups for 12 or 24 h.

The inhibitory growth rates in the AMP, 3-MA, 3-MA + AMP, Z-VAD-FMK, and Z-VAD-FMK + AMP, were (95.84 ± 0.65)%, (7.81 ± 2.82)%, (98.60 ± 0.60)%, (10.42 ± 4.70)% and (97.48 ± 0.56)%, respectively (Table 1). Compared with the AMP group, the number of normal cells decreased slightly in the 3-MA + AMP and Z-VAD-FMK + AMP groups, while the number of broken cells increased (Fig. 7). It implies that autophagy or apoptosis inhibition could promote AMP induced C-33A cell death.

3.5.2 C-33A cell apoptosis was intensified through autophagy inhibition

The control, AMP, 3-MA, and 3-MA + AMP groups were exposed to 3-MA for 2 h before to AMP treatment for 12 h. Compared with the AMP group, Hoechst 33258 staining showed an increased number of apoptotic cells in the 3-MA + AMP group (Fig. 8A), with

Table 1
Identities of the sequenced genes (ITS or 26S rDNA) of yeast strains and the accession numbers of the entries with the highest identity.

Groups	OD	Inhibition rate (%)	OD	Inhibition rate (%)	OD	Inhibition rate (%)
Control	0.322 ± 0.005		0.280 ± 0.011		0.304 ± 0.002	
AMP	0.069 ± 0.002**	95.39	0.066 ± 0.005**	95.55	0.065 ± 0.004**	96.58
3-MA	0.307 ± 0.005**	5.56	0.265 ± 0.004**	6.90	0.277 ± 0.003**	10.98
AMP + 3-MA	0.062 ± 0.003$^{\#\#}$	97.93	0.058 ± 0.005$^{\#\#}$	98.78	0.058 ± 0.005$^{\#\#}$	99.09
Z-VAD-FMK	0.306 ± 0.011	5.93	0.258 ± 0.007	10.02	0.266 ± 0.011**	15.31
AMP + Z-VAD-FMK	0.064 ± 0.005$^{\#\#}$	97.36	0.062 ± 0.005$^{\#\#}$	96.99	0.061 ± 0.005$^{\#\#}$	98.09

Note: $^{**}P < 0.01$ *vs*. Control group; $^{\#\#}P < 0.01$ *vs*. AMP group.

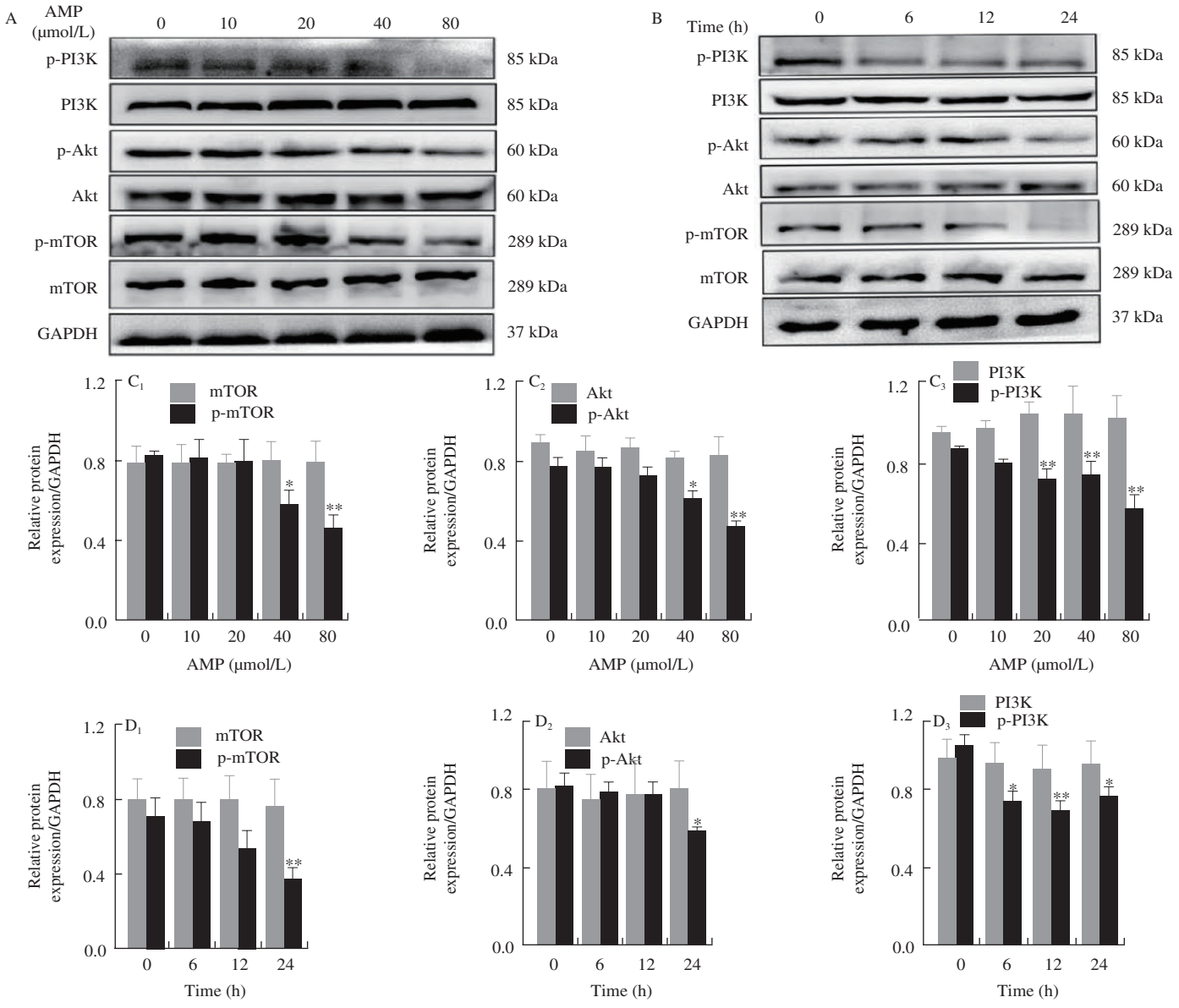

Fig. 6 AMP induces autophagy by suppressing the PI3K/Akt/mTOR pathway in C-33A cells. (A) Levels of PI3K/AKT/mTOR pathway proteins in C-33A cells treated with AMP (0, 10, 20, 40 and 80 μmol/L) for 12 h. (B) Levels of PI3K/AKT/mTOR pathwayproteins in C-33A cells treated with AMP (40 μmol/L) for 0, 6, 12, 24 h. (C) Quantitative analysis of levels of PI3K/AKT/mTOR pathway proteins in C-33A cells treated with different concentration of AMP. (D) Quantitative analysis of levels of PI3K/AKT/mTOR pathway proteins in C-33A cells treated with different time of AMP. Data are represented as the mean ± SD, $n = 3$. $^{*}P < 0.05$; $^{**}P < 0.01$ *vs*. control. ns, not significant.

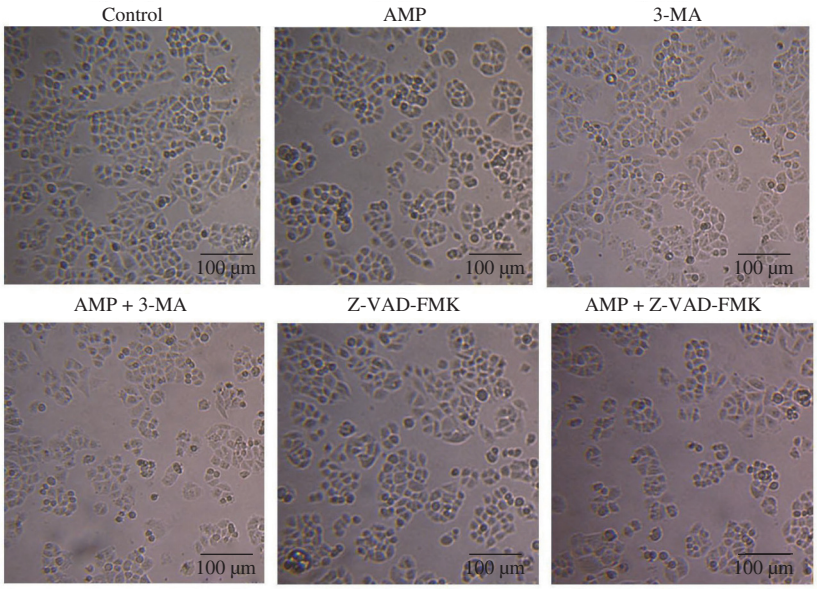

Fig. 7 Effect of AMP and autophagy or apoptosis inhibitors on C-33A cells. Cells were exposed to 3-MA or Z-VAD-FMK for 2 h before adding AMP (40 μmol/L) and addition for 12 h. Scale bar: 100 μm.

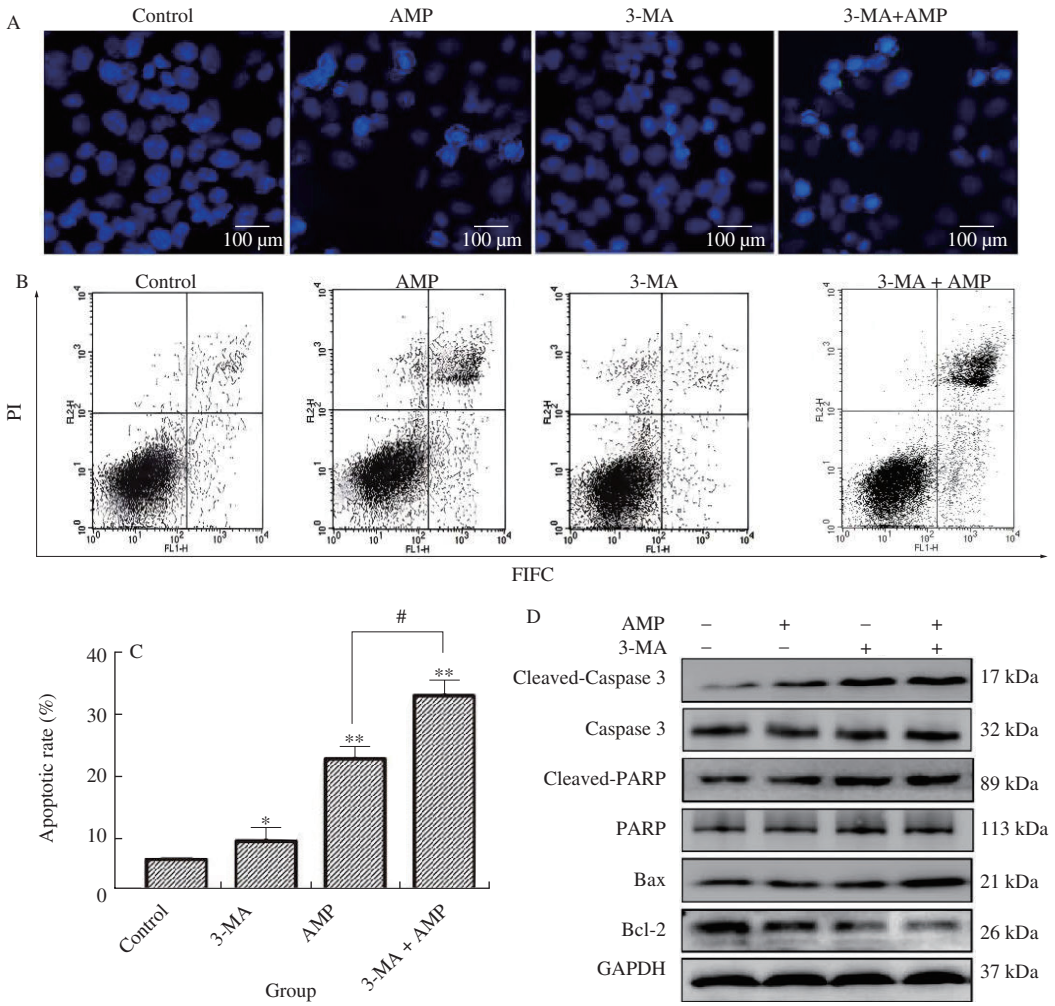

Fig. 8 Treatment with 3-MA inhibits autophagy and promotes apoptosis in C-33A cells. Four groups were set up: control, AMP (40 μmol/L), 3-MA (5 mmol/L), and AMP + 3-MA for 12 h. (A) Hoechst 33258 dyeing was used to measure the typical morphological features of the apoptotic cells. Scale bar: 100 μm. (B-C) Annexin V-FITC/PI dyeing was employed to analyze the cell apoptosis rate. (D) Levels of apoptosis-related proteins were analyzed by Western blot. (E) Levels of Bax/Bcl-2, cleaved-PARP/PARP and cleaved-Caspase 3/Caspase 3 in C-33A cells treated with AMP and 3-MA. Data are represented as the mean ± SD, $n = 3$. $^{*}P < 0.05$; $^{**}P < 0.01$ *vs*. control. $^{\#\#}P < 0.01$ *vs*. AMP. ns, not significant.

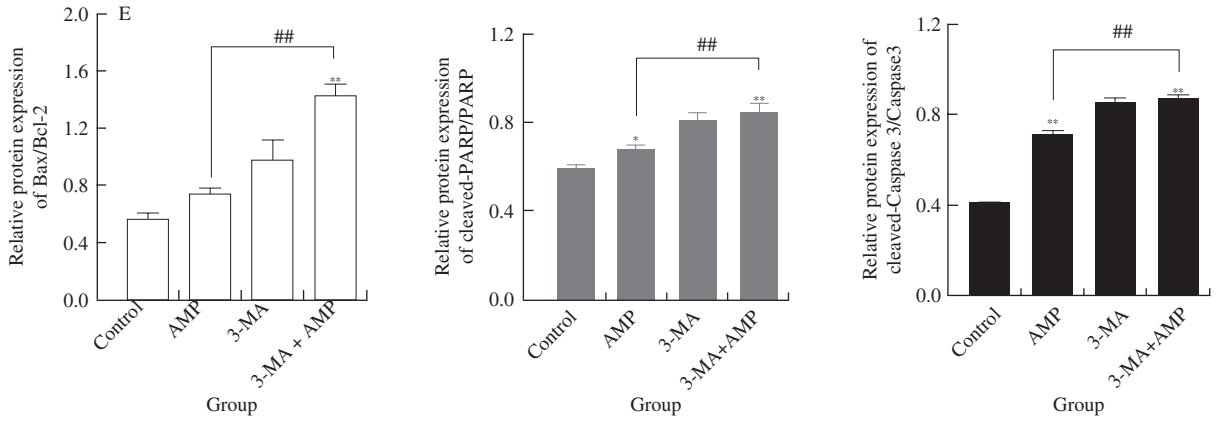

Fig. 8 (*Continued*)

apoptosis rates of (21.92 ± 3.42)% and (32.53 ± 4.84)%, respectively (Figs. 8B and C). Meanwhile, the levels of Bax/Bcl-2, Cleaved-PARP/PARP, and cleaved-Caspase 3/Caspase 3 were up-regulated in the 3-MA + AMP group (Fig. 8D). The findings hint that the AMP-induced apoptosis of C-33A cells was strengthened when autophagy was inhibited.

3.5.3 C-33A cell autophagy was intensified through apoptosis inhibition

Compared with the AMP group, MDC fluorescence staining showed increased green dot fluorescence of autophagosomes in the Z-VAD-FMK + AMP group (Fig. 9A). TEM results further showed that the number of autophagosomes were increased in this group, along with the presence of swollen and denatured mitochondria, and vacuolar structures (Fig. 9B). Furthermore, cells in this group showed increased levels of Beclin 1, LC3 II/LC3 I, and decreased p62 (Fig. 9C). These results reveal that AMP-induced autophagy in C-33A cells were strengthened upon apoptosis inhibition.

3.5.4 Key role of the PI3K/Akt/mTOR pathway in AMP-induced apoptosis and autophagy

Herein, both 3-MA and Z-VAD-FMK were used to research the key factors between autophagy and apoptosis. As shown in Fig. 10, upon autophagy inhibition, the levels of PI3K, Akt and mTOR in the 3-MA + AMP group remained unchanged, while p-PI3K, p-Akt, and p-mTOR levels increased (Fig. 10A). Similarly, upon apoptosis inhibition, the expression of PI3K, Akt, and mTOR in the Z-VAD-FMK + AMP group remained unchanged, while that of p-PI3K, p-Akt, and p-mTOR decreased (Fig. 10B). These findings suggest PI3K/Akt/mTOR pathway activation strengthens AMP-induced apoptosis, while its inhibition strengthens AMP-induced autophagy in C-33A cells.

3.6 AMP inhibits C-33A cell growth in vivo

An xenograft model was established to understand whether we can recapitulate the effects of AMP treatment on C-33A cell proliferation, apoptosis, and autophagy *in vivo*. As shown in Fig. 11, no obvious changes in the body weight and organ coefficients were observed in these mice (Figs. 11A and E). However, the volume of the xenograft increased continuously (Fig. 11B). The average volume of the xenograft was (1 364.65 ± 95.39) mm^3 in the control group, (724.35 ± 57.23) and (685.43 ± 21.06) mm^3 in low-AMP and high-AMP groups, respectively. Compared to the control, the volume inhibition rates for the low-AMP and high-AMP groups were 27.9% and 37.9%, respectively. The DDP group had a volume inhibition rate of 63.44%. The xenograft was also weighed and imaged after removal from the mice (Fig. 11C and D). The weight inhibition rates of the low-, high-, and DDP groups were 20.41%, 39.41%, and 74.04%, respectively. Altogether these results indicated that AMP effectively inhibited xenograft tumor growth and exhibited low toxicity *in vivo*.

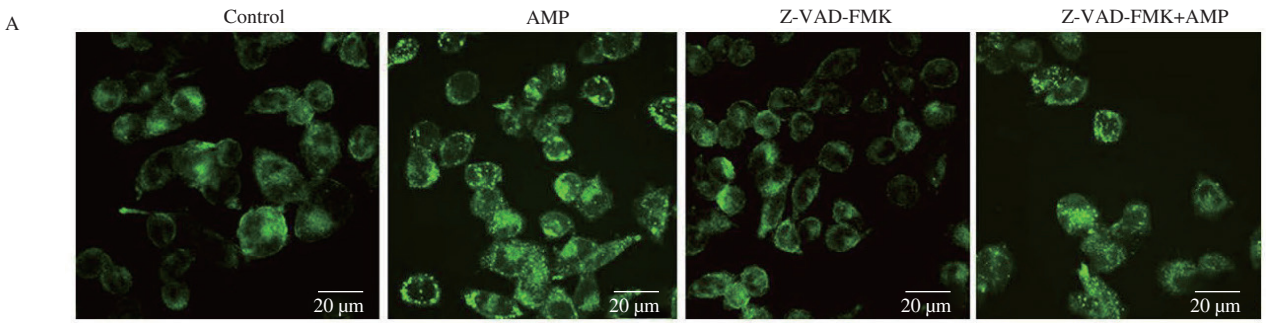

Fig. 9 Treatment with Z-VAD-FMK inhibits apoptosis and promotes autophagy in C-33A cells. Four groups were set up: control, AMP (40 μmol/L), Z-VAD-FMK (50 μmol/L), and AMP + Z-VAD-FMK) for 12 h. (A) Preliminary morphological features of autophagic cells were observed by MDC staining. Scale bar: 20 μm. (B) Typical cell ultrastructures of autophagic cells were observed using TEM. Scale bars: 4, 2 or 1 μm. (C) Levels of autophagy-related proteins were analyzed by Western blot. Data are represented as the mean ± SD, $n = 3$. $^{*}P < 0.05$; $^{**}P < 0.01$ *vs*. control. $^{\#\#}P < 0.01$, *vs*. AMP. ns, not significant.

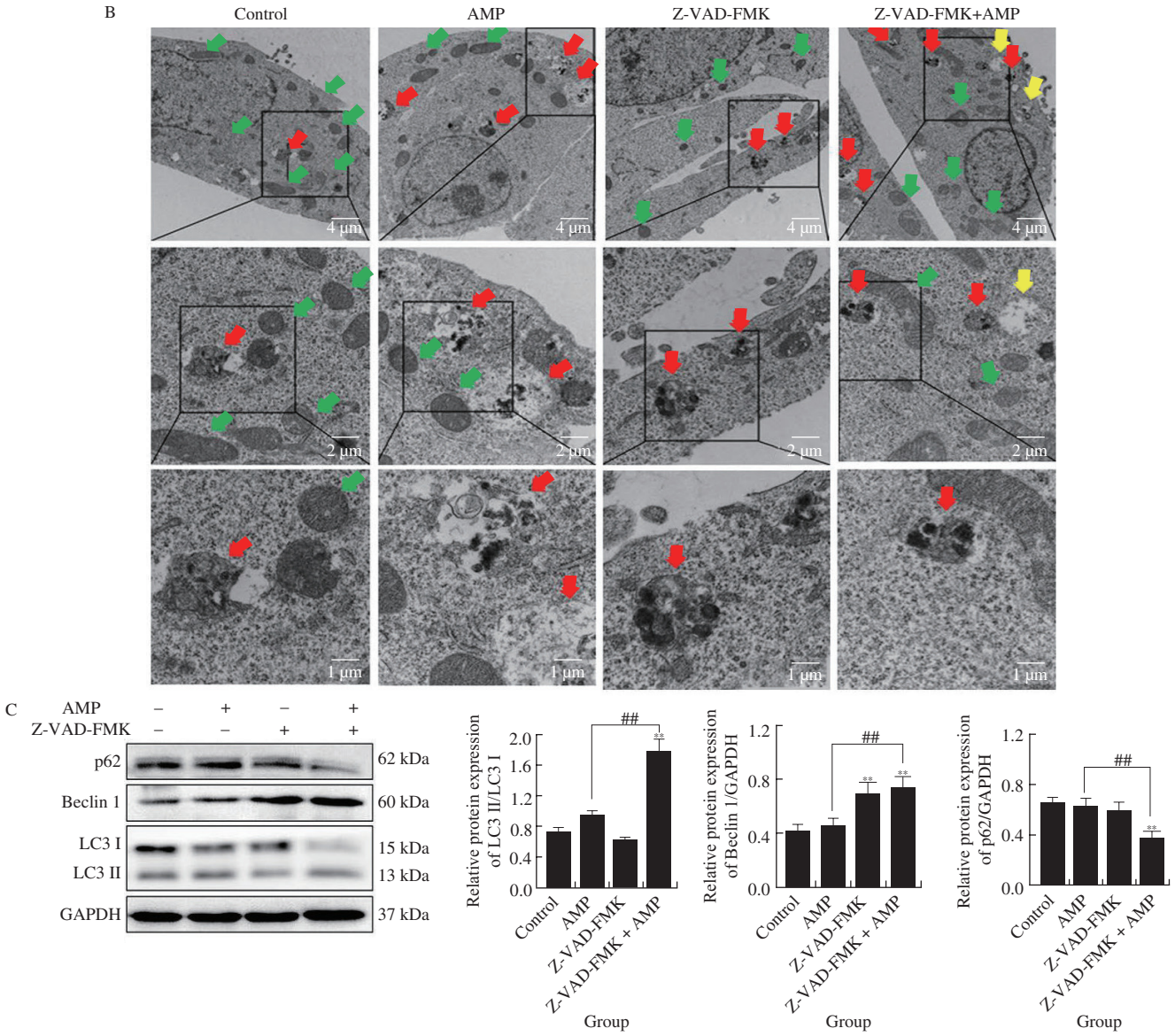

Fig. 9 (*Continued*)

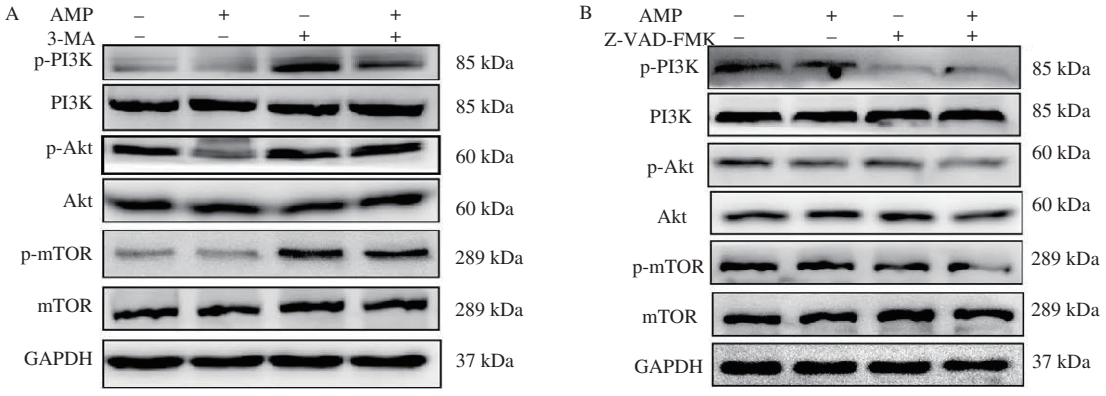

Fig. 10 Protein levels of the PI3K/Akt/mTOR pathway were analyzed by Western blot. (A) Cells were treated according with each group: The Control, AMP, 3-MA, and AMP + 3-MA for 12 h. (B) Cells were treated according with each group: Control, AMP, Z-VAD-FMK, and AMP + Z -VAD -FMK for 12 h. (C) Quantitative analysis of levels of p-mTOR/mTOR, p-PI3K/PI3K and p-AKT/Akt in C-33A cells treated with AMP and 3-MA. (D) Quantitative analysis of levels of p-mTOR/mTOR, p-PI3K/PI3K and p-AKT/Akt in C-33A cells treated with AMP and Z-VAD-FMK. (E) Levels of Bax/Bcl-2, cleaved-PARP/PARP and cleaved-Caspase 3/Caspase 3 in C-33A cells treated with AMP and 3-MA. Data are represented as the mean ± SD, $n = 3$. $^{*}P < 0.05$; $^{**}P < 0.01$ *vs*. control. $^{\#\#}P < 0.01$ *vs*. AMP. ns, not significant.

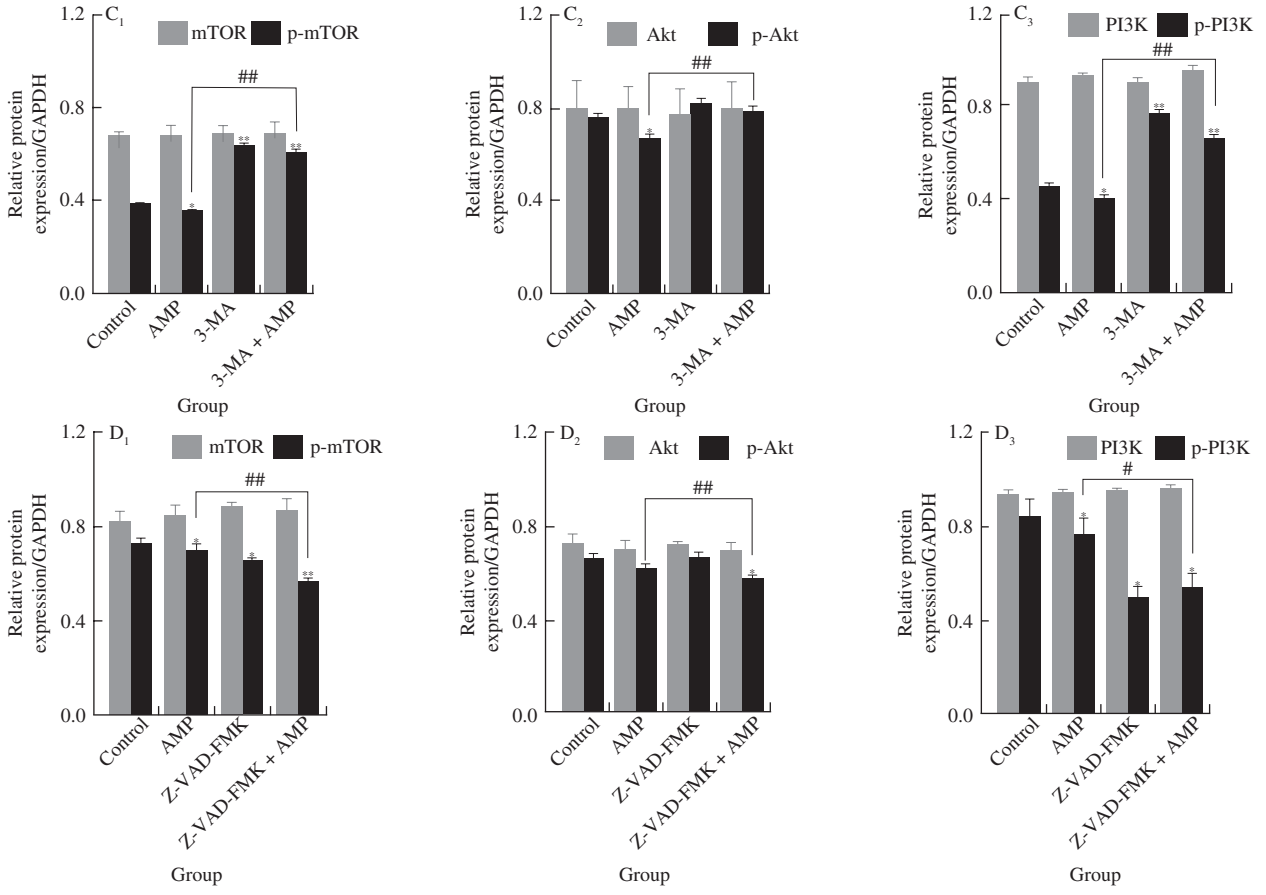

Fig. 10 (*Continued*)

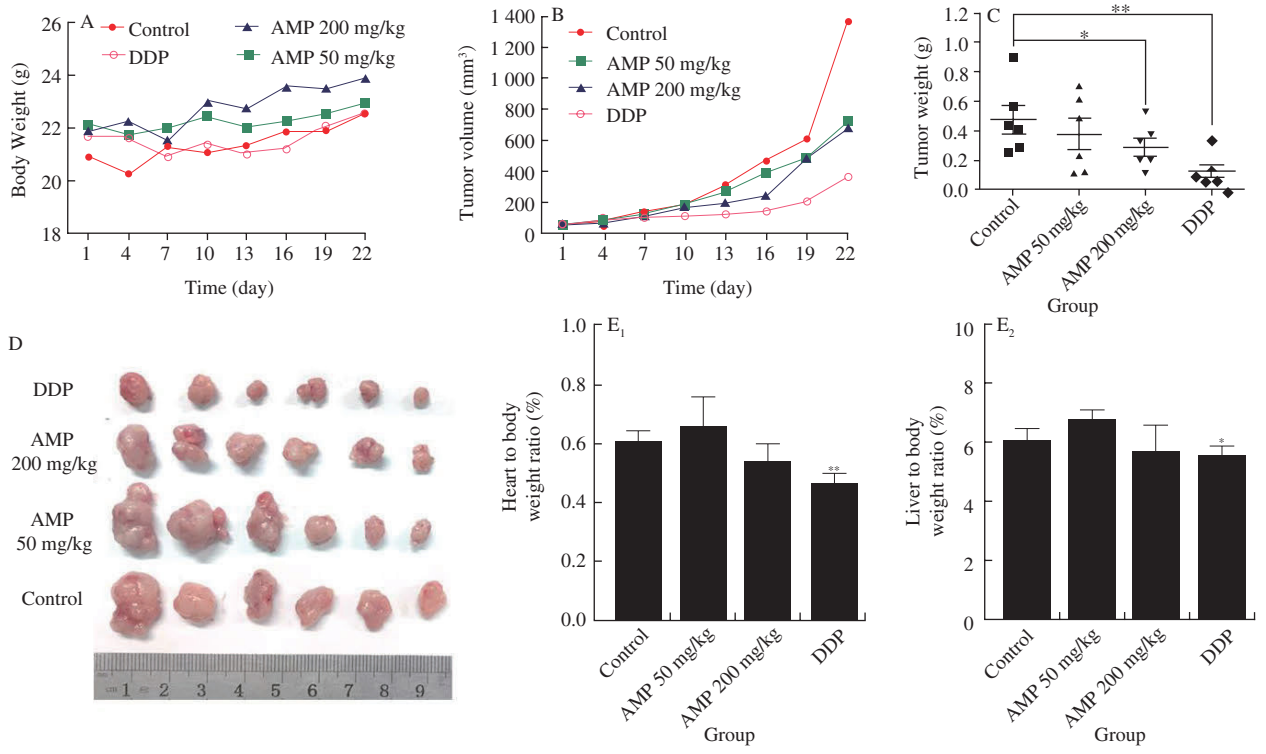

Fig. 11 AMP prevents C-33A xenograft growth *in vivo*. Four groups were included in this study: the control, low-AMP (50 mg/kg), high-AMP (200 mg/kg), and positive control (2.5 mg/kg DDP) groups (n = 6 mice per group). (A) Mice were weighted every 3 days. (B) Xenograft volume was measured every 3 days. (C) Xenograft weights were measured, and the mean was obtained. (D) Photographs of the xenografts. (E) Organ coefficients, including the heart, liver, spleen, lungs, and kidneys. Data are represented as the mean ± SD, n = 6. *P < 0.05; **P < 0.01 *vs*. control. ns, not significant.

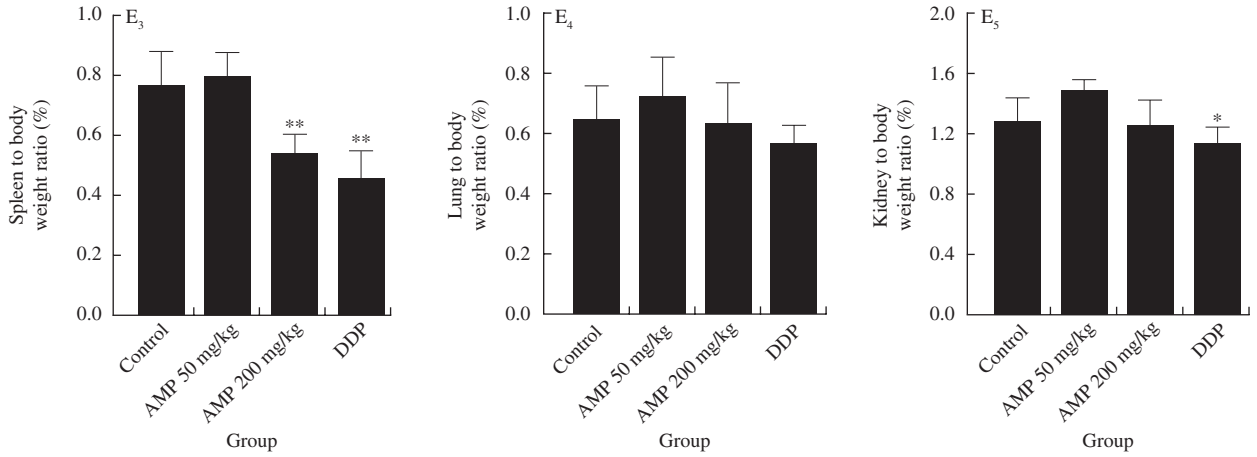

Fig. 11 (*Continued*)

3.7 AMP induces the apoptosis and autophagy of C-33A cell in vivo

The ultrastructure of the xenograft tumors was assessed through TEM. In the low-AMP group, few autophagosomes were present, and the mitochondria had a normal morphology. The number of normal mitochondria and autophagosomes increased significantly in the high-AMP group. There were only few normal mitochondria and several autophagosomes in the DDP group (Fig. 12B). ELISA was employed to test serum levels of TNF-α, IL-6, IL-1β, and IL-2, which were found to be down-regulated upon AMP treatment in a dose-dependent manner (Fig. 12A). RT-qPCR results showed the down-regulation of *Bcl-2* mRNA expression and the up-regulation of *Bax*, *Beclin 1*, and *LC3 II* in both the low- and high-dose groups (Fig. 12C). These results confirmed that AMP induced both apoptosis and autophagy in C-33A cells *in vivo*.

4. Discussion

N. megalophylla is a folk medicinal plant commonly used by the Tujia people in the western Hubei Province of China. Our previous research showed that this plant's extracts had good anticancer effects in the tumor cells lines HeLa, SMMC-7721, A549, and MCF-7, among others[16,25], and that the total flavonoid extract and the main active component, AMP, exhibited an good inhibitory effect on CC cells growth. When HeLa, SiHa and C-33A cells were screened for AMP activity, C-33A cells were found to be the most sensitive to AMP[16,18]. Our result of MTT assay of SiHa and C-33A cells also showed that AMP has a better inhibitory for C-33A cell (Fig. 1). Therefore, C-33A cell was employed to research AMP-induced apoptosis and autophagy and its underlying mechanisms in this study.

The results of Hoechst 33258 single staining, Western blot, and other experiments confirmed that AMP could induce the apoptosis of C-33A cells *in vitro* (Fig. 2). Analyzing the expression of FADD and cytosolic Cyt-c, which were the representative proteins for the 2 forms of apoptosis[8,23], showed that AMP can induce apoiptosis in C-33A cells through the mitochondrial or death receptor pathways (Fig. 3). Other proteins, such as FAS, FAS-L, Caspase 8[26], Caspase 9 and tBid[27], should be explored in future studies to support these data.

Next, we showed that AMP induced autophagy in C-33A cells from the perspective of cell morphology and dynamics using MDC fluorescence staining, TEM, and mRFP-GFP-LC3 autophagy double-labeled adenovirus transfection methods (Figs. 4 and 5). Autophagy is divided into three stages[28], autophagy precursors, autophagosomes, and autophagolysosomes. Briefly, in autophagy,

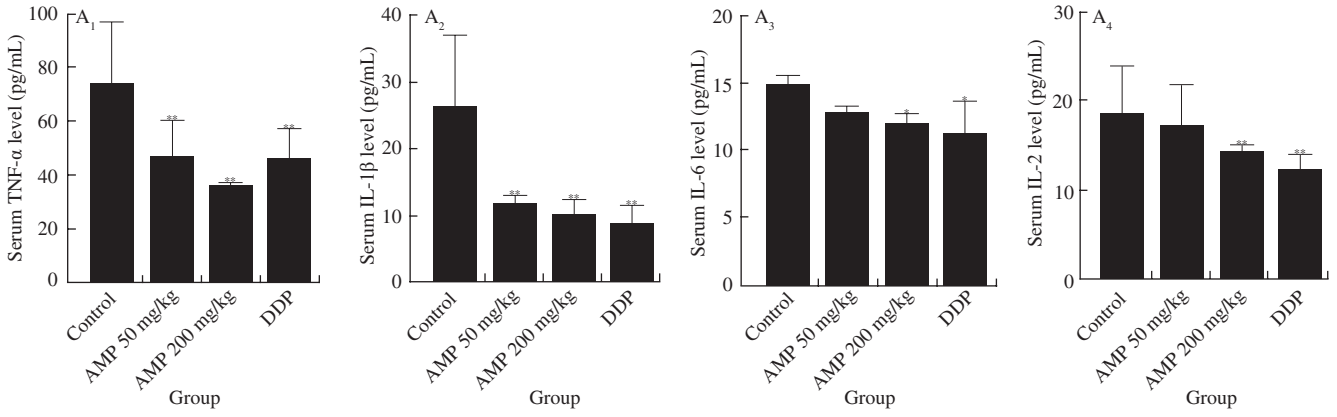

Fig. 12 AMP induces apoptosis and autophagy in C-33A cell *in vivo*. Four groups were included in this study: the control, low-AMP (50 mg/kg), high-AMP (200 mg/kg) and positive control (2.5 mg/kg DDP) groups ($n = 6$ mice per group). (A) Levels serological inflammatory factors, TNF-α, IL-6, IL-1β, and IL-2, were detected by ELISA assay. (B) Typical cell ultrastructure of xenograft tissues was observed using TEM. Scale bars: 4, 2 or 1 μm. (C) RT-qPCR was employed to quantify mRNA expression of *Bax, Bcl-2, Beclin 1* and *LC3 II*. Data are represented as the mean ± SD, $n = 6$. *$P < 0.05$; **$P < 0.01$ *vs*. control. ns, not significant.

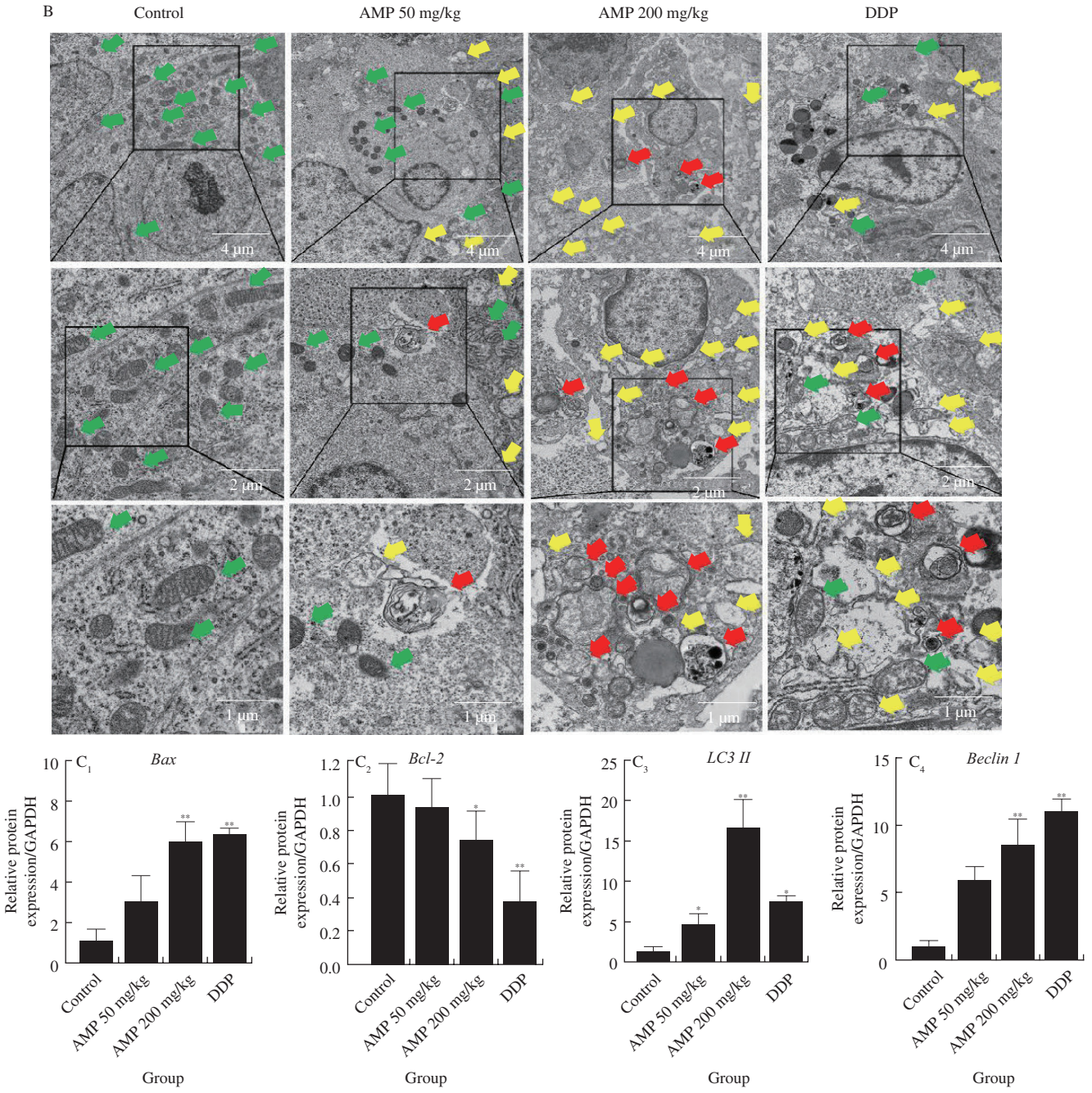

Fig. 12 (*Continued*)

LC3 I is activated by Atg7 and binds to phosphatidylethanolamine on the surface of the autophagy membrane to form LC3 II. Therefore, the expression of both proteins is related to autophagy promotion[29-30]. Beclin 1 interacts with class Ⅲ PI3K to regulate autophagosome formation, thus, its levels are also upregulated during autophagy[31-32]. In contrast, p62 is not only a main player in the degradation of autophagic proteins[33], but it can also bind to ubiquitinated proteins during autophagy, hence, p62 expression gradually decreases. According to reports, since the first confirmed autophagy-related protein in 1996, more than 30 Atg proteins have been discovered[34]. It's important to investigate Atg series proteins[35], which play a vital role in autophagy, expression. In our paper, the upregulation of Atg5 and Atg13 further confirmed that AMP induces autophagy in C-33A cells (Fig. 5). Numerous researches have suggested that the PI3K/Akt/mTOR pathway is inseparable in CC treatment[36]. So the classical signaling pathway of autophagy[37], the PI3K/Akt/mTOR pathway, was studied. In fact, we found that the expression of the phosphorylated forms p-PI3K, p-Akt, and p-mTOR declined while the expression of the base proteins remained unchanged. These studies showed that AMP induces autophagy in C-33A cells *via* the PI3K/Akt/mTOR pathway and that apoptosis occurs concomitantly, suggesting a correlation between apoptosis and autophagy.

Thirdly, according to previous reports, several overlapping mechanisms exist between apoptosis and autophagy. Autophagy is believed to be the leading mechanism of apoptosis, which means

that inhibiting of autophagy can enhance or promote apoptosis. In contrast, other studies suggested that apoptosis inhibition enhances or promotes autophagy[38]. For example, it has been shown that autophagy inhibition, increases the quercetin-induced apoptosis of HeLa cells[39]. Furthermore, chitosan oligosaccharides and docetaxel induce concomitant apoptosis and autophagy in HeLa cells, with Beclin 1 as the bridging factor between processes[40-41]. Thus, autophagy and apoptosis inhibitors, 3-MA and Z-VAD-FMK, were used to explore the interaction between these 2 modes of cell death.

We employed previously reported methods to elucidate the activity of autophagy inhibition on apoptosis and vice versa. On the one hand, our results suggested that inhibition of autophagy can promote apoptosis and the PI3K/Akt/mTOR pathway is activated (Figs. 8 and 10A). On the other hand, our findings also indicated that inhibition of apoptosis can promote autophagy, and the PI3K/Akt/mTOR pathway is inhibited (Figs. 9 and 10B). Thus, there was an antagonistic relationship between AMP-induced apoptosis and autophagy in C-33A cells. Furthermore, studies found that the PI3K/Akt/mTOR pathway has anti-apoptotic effects[42].

Finally, cell lines cannot accurately simulate the complex tumor microenvironment. Therefore, we established a model by implanting a subcutaneous xenograft of CC tumor cells (C-33A) in immunodeficient nude mice. We used this model to understand whether we could recapitulate *in vivo* the inhibitory action of AMP on C-33A cells growth, and evaluate apoptosis and autophagy. The body weight changes of nude mice during the administration period indicated that the toxicity of AMP was low and had little effect on the normal growth of mice (Fig. 11A), which was consistent with previous reports[43]. AMP has also been reported to have high safety profile[21]. The weight and volume of the xenograft tumor are directly correlated to cell growth and proliferation. We found that the volume inhibition rate of the positive control group was the highest, followed by the high-AMP and the low-AMP group. The same effect was observed suppress the growth of C-33A xenografts. Subsequently, we explored the mechanisms through that AMP restrains the growth of C-33A xenografts *via* apoptosis and autophagy.

TNF-α is a multifunctional cytokine with a direct antitumor effect, showing low expression under normal circumstances. However, inflammation, infection, and external stimuli cause TNF-α release[44]. The caspase family and apoptosis-related proteins are divided into 3 categories: apoptosis-initiating factors, apoptosis-executing factors, and inflammatory mediators, which constitute a cascade effect. Autophagy can inhibit tumor cell proliferation by inhibiting inflammation, preventing tumor cell necrosis, and removing the cytoskeletal protein p62, etc.[45- 46]. Therefore, both apoptosis and autophagy are related to inflammatory factors. Indeed, AMP was shown to reduce the levels of TNF-α, IL-2, IL-1β, and IL-6 (Fig. 12A). Taken together, AMP may inhibit the growth of xenografted tumors through autophagy or apoptosis.

The TEM experiments also showed AMP-induced autophagy occurrence in the tumor xenografts, supported by the increased mRNA expressions of *Beclin 1* and *LC3 II* (Figs. 12B and C), which were in agreement with the *in vitro* results (Figs. 4 and 5). mRNA levels of *Bcl-2* decreased, and that of *Bax* increased, indicating that autophagy might be occurring at the same time as apoptosis. Thus, we showed that AMP also induces apoptosis and autophagy *in vivo*. The entire signaling pathway suggested by our experiments is shown in Fig. 13.

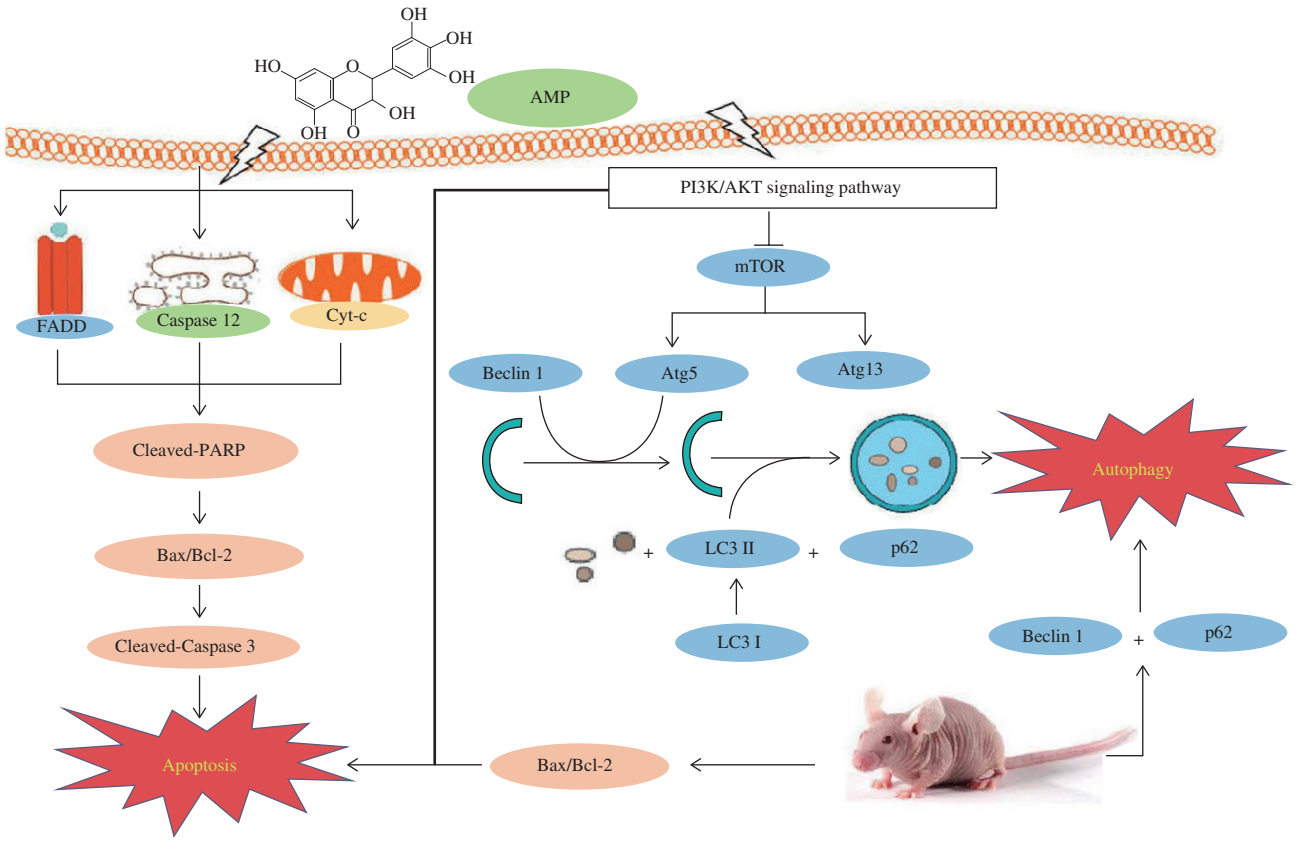

Fig. 13 AMP-induced inhibition of the human cervical cancer C-33A cell line, regulating autophagy and apoptosis *in vitro* and *in vivo*.

5. Conclusion

In summary, we reported the anti-CC mechanism of AMP and explored the relationship between apoptosis and autophagy for the first time in the context. We also reported the mechanism of AMP action on C-33A cells from both *in vitro* and *in vivo*, showing the interrelatedness between cell proliferation, apoptosis, and autophagy. Our results showed thar the apoptotic and autophagic processes are mutually antagonistic and that the PI3K/Akt/mTOR pathway is probably the key factor in this relationship. Hence, natural AMP extract is a potential drug for CC treatment, and we will screen direct targets of AMP for targeted clinical research in the future.

Conflict of interest

The authors declare that they have no known competing financial interests or personal relationships that could have appeared to influence the work reported in this paper.

Acknowledgements

This work was supported by the Major Science and Technology Project of Hubei Province (2020ACA007) and the Scientific and Technological Bureau of Wuhan (2018060401011308).

Institutional review board statement

The experimental procedures were approved by the Animal Experimentation Ethics Committee of the Hubei University of Chinese Medicine and conformed to the guidelines of the "Principles of Laboratory Animal Care" (NIH publication No. 80-23, revised 1996).

Appendix A. Supplementary data

Supplementary data associated with this article can be found, in the online version, at http://doi.org/10.26599/FSHW.2024.9250359.

References

[1] H. Sung, J. Ferlay, R.L. Siegel, et al., Global Cancer Statistics 2020: GLOBOCAN estimates of incidence and mortality worldwide for 36 cancers in 185 countries, CA Cancer. J. Clin. 71 (2021) 209-249. https://doi.org/10.3322/caac.21660.

[2] F. Bray, B. Carstensen, H. Moller, et al., Incidence trends of adenocarcinoma of the cervix in 13 European countries, Cancer Epidem Biomar. 14 (2005) 2191-2199. https://doi.org/10.1158/1055-9965.EPI-05-0231.

[3] J.M. Lemp, J.W. De Neve, H. Bussmann, et al., Lifetime prevalence of cervical cancer screening in 55 low- and middle-income countries, JAMA 324 (2020) 1532-1542. https://doi.org/10.1001/jama.2020.16244.

[4] C.A. Johnson, D. James, A. Marzan, et al., Cervical cancer: an overview of pathophysiology and management, Semin. Oncol. Nurs. 35 (2019) 166-174. https://doi.org/10.1016/j.soncn.2019.02.003

[5] K.K. Vesco, E.P. Whitlock, M. Eder, et al., Risk factors and other epidemiologic considerations for cervical cancer screening: a narrative review for the U.S. Preventive Services Task Force, Ann. Intern. Med. 155 (2011) 698-705. https://doi.org/10.7326/0003-4819-155-10-201111150-00377.

[6] Z. Zou, C.K. Fairley, J.J. Ong, et al., Domestic HPV vaccine price and economic returns for cervical cancer prevention in China: a cost-effectiveness analysis, Lancet Glob. Health 8 (2020) e1335-e1344. https://doi.org/10.1016/S2214-109X(20)30277-1.

[7] M. Liontos, A. Kyriazoglou, I. Dimitriadis, et al., Systemic therapy in cervical cancer: 30 years in review, Crit. Rev. Oncol. Hemat. 137 (2019) 9-17. https://doi.org/10.1016/j.critrevonc.2019.02.009.

[8] D.J. Newman, G.M. Cragg, Natural products as sources of new drugs over the nearly four decades from 01/1981 to 09/2019, J. Nat. Prod. 83 (2020) 770-803. https://doi.org/10.1021/acs.jnatprod.9b01285.

[9] N.S. Yarla, A. Bishayee, G. Sethi, et al., Targeting arachidonic acid pathway by natural products for cancer prevention and therapy, Semin. Cancer Biol. 40-41 (2016) 48-81. https://doi.org/10.1016/j.semcancer.2016.02.001.

[10] A. Hazafa, K.U. Rehman, N. Jahan, et al., The role of polyphenol (flavonoids) compounds in the treatment of cancer cells, Nutr. Cancer. 72 (2020) 386-397. https://doi.org/10.1080/01635581.2019.1637006.

[11] G. Qin, P. Li, Z. Xue, Triptolide induces protective autophagy and apoptosis in human cervical cancer cells by downregulating Akt/mTOR activation, Oncol Lett. 16 (2018) 3929-3934. https://doi.org/10.3892/ol.2018.9074.

[12] Y. Liu, H. Li, Z. Zheng, et al., *Rosa rugosa* polysaccharide induces autophagy-mediated apoptosis in human cervical cancer cells *via* the PI3K/AKT/mTOR pathway, Int. J. Biol. Macromol. 212 (2022) 257-274. https://doi.org/10.1016/j.ijbiomac.2022.05.023.

[13] S. Huang, T. Xie, W. Liu, Icariin inhibits the growth of human cervical cancer cells by inducing apoptosis and autophagy by targeting mTOR/PI3K/AKT signalling pathway, J. Buon. 24 (2019) 990-996.

[14] J.P. Tsai, C.H. Lee, T.H. Ying, et al., Licochalcone A induces autophagy through PI3K/Akt/mTOR inactivation and autophagy suppression enhances licochalcone A-induced apoptosis of human cervical cancer cells, Oncotarget 6 (2015) 28851-28866. https://doi.org/10.18632/oncotarget.4767.

[15] P. Cheng, C. Gui, J. Huang, et al., Molecular mechanisms of ampelopsin from *Nekemias megalophylla* induces apoptosis in HeLa cells, Oncol. Lett. 14 (2017) 2691-2698. https://doi.org/10.3892/ol.2017.6520.

[16] T. Zeng, Y. Song, S. Qi, et al., A comprehensive review of vine tea: origin, research on Materia Medica, phytochemistry and pharmacology, J. Ethnopharmacol. 5 (2023) 116788. https://doi.org/10.1016/j.jep.2023.116788.

[17] C. Gui, J. Huang, P. Cheng, et al., Screening of anti-tumor active substances from Ampelopsis grossedentata *in vitro*, Chinese Patent Medicine 37 (2015) 1411-1416.

[18] J. Fang, C. Gui, C. Zhang, et al., Effect of ampelopsin on proliferation, cell cycle and apoptosis of human cervical carcinoma SiHa cells, Chinese Pharmacological Bulletin 37 (2021) 83-89.

[19] X. Kou, J. Fan, N. Chen, Potential molecular targets of ampelopsin in prevention and treatment of cancers, Anti-Cancer Agent Me. 17 (2017) 1610-1616. https://doi.org/10.2174/1871521409666170412130529.

[20] X. Li, Z.S. Yang, W.W. Cai, et al., Dihydromyricetin inhibits tumor growth and epithelial-mesenchymal transition through regulating miR-455-3p in cholangiocarcinoma, J. Cancer 12 (2021) 6058-6070. https://doi.org/10.7150/jca.61311.

[21] Z. Zhao, Y. Jiang, Z. Liu, et al., Ampelopsin inhibits cell viability and metastasis in renal cell carcinoma by negatively regulating the PI3K/AKT signaling pathway, Evid-Based Compl. Alt. 2021 (2021) 4650566. https://doi.org/10.1155/2021/4650566.

[22] K. Ranjan, B.N. Waghela, F.U. Vaidya, et al., Cell-penetrable peptide-ponjugated FADD induces apoptosis and regulates inflammatory signaling in cancer cells, Int. J. Mol. Sci. 21(18) (2021) 6890. https://doi.org/10.3390/ijms21186890.

[23] Y. Jin, S. Zhang, R. Tao, et al., Oral exposure of mice to cadmium (II), chromium (VI) and their mixture induce oxidative- and endoplasmic reticulum-stress mediated apoptosis in the livers, Environ. Toxicol. 31 (2016) 693-705. https://doi.org/10.1002/tox.22082.

[24] D.J. Klionsky, G. Petroni, R.K. Amaravadi, et al., Autophagy in major human diseases, EMBO J. 40 (2021) e108863. https://doi.org/10.15252/embj.2021108863.

[25] C. Gui, C. Zhang, X. Xiong, et al., Total flavone extract from *Nekemias megalophylla* induces apoptosis in the MCF-7 cell line, Int. J. Oncol. 58 (2021) 409-418. https://doi.org/10.3892/ijo.2021.5172.

[26] Y. Sekiguchi, M. Yamada, T. Noguchi, et al., The anti-cancer drug gefitinib accelerates Fas-mediated apoptosis by enhancing Caspase-8 activation in cancer cells, J. Toxicol. Sci. 44 (2019) 435-440. https://doi.org/10.2131/jts.44.435.

[27] Y. Rellmann, E. Eidhof, R. Dreier, Review: ER stress-induced cell death in osteoarthritic cartilage, Cell Signal. 78 (2021) 109880. https://doi.org/10.1016/j.cellsig.2020.109880.

[28] T. Ichimiya, T. Yamakawa, T. Hirano, et al., Autophagy and autophagy-related diseases: a review, Int. J. Mol. Sci. 21(23) (2020) 8974. https://doi.org/10.3390/ijms21238974.

[29] X. Chen, Y. Sun, B. Wang, et al., Prognostic significance of autophagy-related genes *Beclin1* and *LC3* in ovarian cancer: a meta-analysis, J. Int. Med. Res. 48 (2020) 1220767851. https://doi.org/10.1177/0300060520968299.

[30] Y. Deng, Q.S. Chen, W.F. Huang, et al., XPA serves as an autophagy and apoptosis inducer by suppressing hepatocellular carcinoma in a PI3K/Akt/mTOR dependent manner, J. Gastrointest. Oncol. 12 (2021) 1797-1810. https://dx.doi.org/10.21037/jgo-21-310.

[31] Y. Liu, A. Song, H. Wu, et al., Paeonol inhibits apoptosis of vascular smooth muscle cells *via* up-regulation of autophagy by activating class III PI3K/Beclin 1 signaling pathway, Life Sci. 264 (2021) 118714. https://doi.org/10.1016/j.lfs.2020.118714.

[32] X. Xie, C. Chen, C.B. Xu, et al., The Class III PI3K/Beclin 1 autophagic pathway participates in the mmLDL-Induced upregulation of ET(A) receptor in mouse mesenteric arteries, Adv. Pharm. Pharm. Sci. 2020 (2020) 5070436. https://doi.org/10.1155/2020/5070436.

[33] H. Jin, Q. Wu, G. Kroemer, et al., A fluorescence-microscopic system for monitoring the turnover of the autophagic substrate p62/SQSTM1, Methods Mol. Biol. 2543 (2022) 71-82. https://doi.org/10.1007/978-1-0716-2553-8_7.

[34] Y. Luo, C. Jiang, L. Yu, et al., Chemical biology of autophagy-related proteins with posttranslational modifications: from chemical synthesis to biological applications, Front. Chem. 8 (2020) 233. https://doi.org/10.3389/fchem.2020.00233.

[35] S. Li, J. Xu, X. Xu, et al., Functional identification of *Bombyx mori* Atg13 in autophagy, Arch. Insect Biochem. 105 (2020) e21718. https://doi.org/10.1002/arch.21718.

[36] L. Fu, W. Wu, X. Sun, et al., Glucocorticoids enhanced osteoclast autophagy through the PI3K/Akt/mTOR signaling pathway, Calcified Tissue Int. 107 (2020) 60-71. https://doi.org/10.1007/s00223-020-00687-2.

[37] J. Long, X. Pi, Polyphyllin I promoted melanoma cells autophagy and apoptosis *via* PI3K/Akt/mTOR signaling pathway, Biomed. Res. Int. 2020 (2020) 5149417. https://doi.org/10.1155/2020/5149417.

[38] W. Xin, J.K. Daniel, At a glance: a history of autophagy and cancer, Semin. Cancer Biol. 66 (2019) 3-11. https://doi.org/10.1016/j.semcancer.2019.11.005.

[39] E.J. Ha, K.Y. Kim, C.E. Kim, et al., Enhancement of quercetin-induced apoptosis by cotreatment with autophagy inhibitor is associated with augmentation of BAK-dependent mitochondrial pathway in Jurkat T Cells, Oxid. Med. Cell Longev. 2019 (2019) 7989276. https://doi.org/10.1155/2019/7989276.

[40] S. Bian, Y. Zhao, F. Li, et al., 20(*S*)-Ginsenoside Rg3 promotes HeLa cell apoptosis by regulating autophagy, Molecules 24(20) (2019) 3655. https://doi.org/10.3390/molecules24203655.

[41] F. Liu, Q. Hu, Z. Ji, Autophagy induced apoptosis of cervical cancer HeLa cells induced by docetaxel, Chinese Journal of Clinical Pharmacology and Therapeutics 14 (2009) 877-882.

[42] Z. Yao, X. Zhang, J. Guo, et al., Gematone activates AMPK and induces autophagy and apoptosis in Hela cells, Chin. J. Immunol. 36 (2020) 2105-2108.

[43] Z. Gao, Z. Li, Cotinine promotes the occurrence of non-small cell lung cancer by activating the anti apoptotic effect of PI3K/Akt pathway, Chinese Journal of Medicine and Clinical Sciences 19 (2019) 4246-4248.

[44] Y. Wang, M. Chen, J. Xin, et al., The role of IL-1β and TNF-α in intervertebral disc degeneration, Biomed. Pharmacother. 131 (2020) 110660. https://doi.org/10.1016/j.biopha.2020.110660.

[45] C. Jiao, G. Zheng, J. Fu, et al., Research progress of Cyt-c and Caspase families and apoptosis of facial neurons, China Clinical Research 34 (2021) 1268-1271.

[46] Y. Tu, B. Tan, L. Jiang, et al., Emodin inhibits lipopolysaccharide-induced inflammation by activating autophagy in RAW 264.7 cells, Chin. J. Integr. Med. 27 (2021) 345-352. https://doi.org/10.1007/s11655-020-3477-9.